2018

Sarcosine is uniquely modulated by aging and dietary restriction in rodents and humans

Valeria Tosti
Washington University School of Medicine in St. Louis
Luigi Fontana
Washington University School of Medicine in St. Louis
et al

Article

Cell Reports

Sarcosine Is Uniquely Modulated by Aging and Dietary Restriction in Rodents and Humans

Graphical Abstract

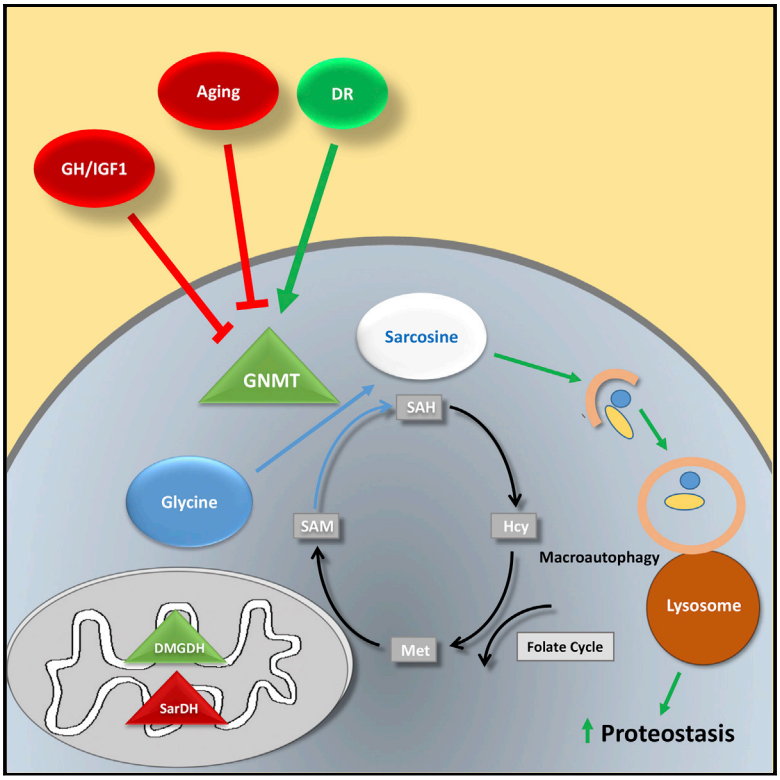

Highlights

- Dietary restriction is a stronger modulator of the rat metabolome than age
- Sarcosine is similarly decreased by age and increased by DR in rodents and humans
- Sarcosine is elevated in serum of long-lived Ames dwarf mice
- Sarcosine activates macroautophagy *in vitro* and *in vivo*

Authors

Ryan O. Walters, Esperanza Arias, Antonio Diaz, ..., Ana Maria Cuervo, Daniel E.L. Promislow, Derek M. Huffman

Correspondence

derek.huffman@einstein.yu.edu

In Brief

In a comparative metabolic screen of rodents and humans, Walters et al. show that circulating sarcosine is similarly reduced with aging and increased by dietary restriction. They demonstrate that sarcosine activates macroautophagy in cultured cells and *in vivo*, suggesting a role in improved proteostasis via dietary restriction.

Walters et al., 2018, Cell Reports *25*, 663–676
October 16, 2018
https://doi.org/10.1016/j.celrep.2018.09.065

CellPress

Cell Reports
Article

Sarcosine Is Uniquely Modulated by Aging and Dietary Restriction in Rodents and Humans

Ryan O. Walters,[1,2,7] Esperanza Arias,[2,7] Antonio Diaz,[4,7] Emmanuel S. Burgos,[5] Fangxia Guan,[2,7] Simoni Tiano,[4,7] Kai Mao,[1,2,7] Cara L. Green,[8] Yungping Qiu,[2,6] Hardik Shah,[2,6] Donghai Wang,[1,7] Adam D. Hudgins,[3] Tahmineh Tabrizian,[1,7] Valeria Tosti,[11] David Shechter,[5] Luigi Fontana,[9,10,11,12] Irwin J. Kurland,[2,6] Nir Barzilai,[2,3,7] Ana Maria Cuervo,[4,7] Daniel E.L. Promislow,[13,14] and Derek M. Huffman[1,2,7,15,*]

[1]Department of Molecular Pharmacology, Albert Einstein College of Medicine, Bronx, NY, USA
[2]Department of Medicine, Albert Einstein College of Medicine, Bronx, NY, USA
[3]Department of Genetics, Albert Einstein College of Medicine, Bronx, NY, USA
[4]Department of Developmental and Molecular Biology, Albert Einstein College of Medicine, Bronx, NY, USA
[5]Department of Biochemistry, Albert Einstein College of Medicine, Bronx, NY, USA
[6]Einstein-Mount Sinai Diabetes Research Center, Stable Isotope and Metabolomics Core Facility, Albert Einstein College of Medicine, Bronx, New York, USA
[7]Institute for Aging Research, Albert Einstein College of Medicine, Bronx, NY, USA
[8]Institute of Biological and Environmental Sciences, University of Aberdeen, Aberdeen, Scotland, UK
[9]Charles Perkins Centre, The University of Sydney, NSW 2006, Australia
[10]Central Clinical School, The University of Sydney, NSW 2006, Australia
[11]Department of Medicine, Washington University School of Medicine, St. Louis, MO 63110, USA
[12]Department of Clinical and Experimental Sciences, Brescia University Medical School, Brescia, Italy
[13]Department of Pathology, University of Washington, Seattle, WA, USA
[14]Department of Biology, University of Washington, Seattle, WA, USA
[15]Lead Contact
*Correspondence: derek.huffman@einstein.yu.edu
https://doi.org/10.1016/j.celrep.2018.09.065

SUMMARY

A hallmark of aging is a decline in metabolic homeostasis, which is attenuated by dietary restriction (DR). However, the interaction of aging and DR with the metabolome is not well understood. We report that DR is a stronger modulator of the rat metabolome than age in plasma and tissues. A comparative metabolomic screen in rodents and humans identified circulating sarcosine as being similarly reduced with aging and increased by DR, while sarcosine is also elevated in long-lived Ames dwarf mice. Pathway analysis in aged sarcosine-replete rats identify this biogenic amine as an integral node in the metabolome network. Finally, we show that sarcosine can activate autophagy in cultured cells and enhances autophagic flux *in vivo*, suggesting a potential role in autophagy induction by DR. Thus, these data identify circulating sarcosine as a biomarker of aging and DR in mammalians and may contribute to age-related alterations in the metabolome and in proteostasis.

INTRODUCTION

An overall decline in metabolic homeostasis is a hallmark of aging across mammalian species (Barzilai et al., 2012). We and others have shown that visceral and ectopic fat accrual, subcutaneous fat depletion, hyperlipidemia, and insulin resistance are characteristic age-related changes in rodents and humans (Barzilai et al., 2012; Cartier et al., 2009; Johannsen et al., 2012). In spite of these well-recognized gross metabolic manifestations, our understanding of how shifts in specific metabolites and pathways are affected by aging, as well as by age-delaying strategies such as dietary restriction (DR), has only recently begun to be elucidated.

An early metabolomic study using 4- and 22-month-old male C57BL/6 mice reported that aging was characterized by altered glucose and fatty acid metabolism, including a lower respiratory exchange ratio (RER), increased plasma fatty acids, and reductions in triglycerides (TGs), various amino acids, and acylcarnitines (Houtkooper et al., 2011). In another study using older female C57BL/6 mice, it was reported that DR opposed a significant number of identified age-related changes in lipid metabolism, fatty acid metabolism, and bile acid biosynthesis (De Guzman et al., 2013), suggesting that at least some age-related shifts in the metabolome can be prevented.

The metabolomic profile of aging has also been assessed in a number of other species, including *Drosophila melanogaster* (Hoffman et al., 2014), naked mole rat (Mitchell et al., 2007), marmoset (Hoffman et al., 2016), and humans (Cheng et al., 2015). Tissue-specific metabolomic signatures were reported to correlate with body mass and lifespan across a diverse number of species, and some tissue metabolites were found that discriminated long-lived rodents from controls (Ma et al., 2015). Although data on metabolomic shifts with aging and diet

are rapidly accumulating, replication across studies has been limited, which has slowed progress toward ascertaining consensus hallmark candidates and signatures that define the aging metabolome across sex, strain, and species. Furthermore, to what extent these metabolomic shifts are merely a consequence of aging per se, as opposed to playing a causal role in the aging process, has been difficult to discern from what has largely been observational data.

Here, we have characterized changes in the metabolome with aging and DR using established techniques in plasma and multiple tissues from a well-characterized hybrid rat model of aging. We have also interrogated the metabolome for shared changes in a set of human samples obtained from a cohort of younger and older subjects consuming a Western or DR diet (Meyer et al., 2006; Soare et al., 2011; Stein et al., 2012). We report on some unique shifts in the metabolome, including alterations in glycerophospholipids, biogenic amines, and amino acids with diet and age. In addition, statistical analyses revealed that DR is a stronger driver of the circulating and tissue rat metabolomic phenotype than age.

When screening for metabolites with similar responses between species, we identified circulating sarcosine, a biogenic amine involved in methionine (Met), glycine, and folate metabolism, as decreased with aging per se in rodents and humans and increased by DR in both species. These shifts correlated with changes in rat liver glycine-*N*-methyltransferase (GNMT) content, which is a known sarcosine-generating enzyme. Long-lived Ames dwarf mice demonstrate significantly elevated sarcosine levels across age, while correlation analysis of metabolites following sarcosine refeeding in old rats prominently places this metabolite as an integral node linking amines, amino acids, glycerophospholipids, and sphingolipids. We also show that sarcosine feeding reduces Met levels in old animals and is a strong activator of macroautophagy *in vitro* and *in vivo*. Taken together, these data identify sarcosine as a potentially important biomarker of diet and aging in mammals and suggest that this metabolite plays a previously unappreciated role in mediating at least some of the beneficial effects attributed to DR on proteostasis.

RESULTS

DR Is a Stronger Modulator of the Rat Metabolic Phenotype than Age

We first characterized the metabolic phenotype of young and old *ad libitum* (AL) and DR Fischer 344 × Brown Norway (FBN) male rats (abbreviated YAL, OAL, YDR, and ODR, respectively) (Figure 1). OAL animals had increased body mass with age and weighed more than age-matched DR rats (Figure 1A; $p < 0.05$), along with a tendency toward greater amounts of lean body mass (Figure 1B; age $p = 0.025$, diet $p < 0.001$, interaction $p = 0.098$) and adiposity (Figure 1C; $p < 0.05$). By design, DR animals consumed 40% fewer calories than AL animals (Figure 1D; age $p = 0.18$, diet $p < 0.001$, interaction $p = 0.18$) and had a lower absolute energy expenditure (EE) (Figure 1E; age $p = 0.082$, diet $p < 0.001$, interaction $p = 0.69$), while 24 hr EE was maintained at youthful levels after adjusting for lean body mass (LBM) (Figure 1F; interaction $p = 0.029$). Substrate utilization in FBN rats was modulated over time by aging (age × time $p = 0.019$) and diet (diet × time $p < 0.001$), as demonstrated by disparate substrate utilization between AL and DR animals, particularly during the dark phase (Figure 1G, red box). In response to an overnight fast, YAL and OAL animals demonstrated a rapid and significant fall in RER (<0.7), suggesting a severe shift away from carbohydrate utilization and heavy reliance on fat and ketone metabolism, while DR animals were better able to handle this provocation, irrespective of age (Figure 1G, green box; $p < 0.05$). No difference in spontaneous activity (Figure 1H) or plasma glucose (Figure 1I) was observed, but OAL animals tended to be hyperinsulinemic (Figure 1J; age $p < 0.001$, diet $p < 0.001$, interaction $p = 0.40$) and had increased plasma TGs (Figure 1K; $p < 0.05$). Free fatty acid (FFA) levels were similar (Figure 1L). However, glycerol was increased in YDR as compared to YAL animals, while ODR animals demonstrated lower levels than controls (Figure 1M; $p < 0.05$).

Effect of Aging and DR on the Circulating and Tissue Metabolome

We next assessed changes at the level of the metabolome with aging and DR in rat plasma, brown adipose tissue (BAT), skeletal muscle (SkM), and liver as well as human serum. Specifically, we compared the slopes of age and diet on all metabolite levels, as determined by the β values obtained from Equation 1 (see Method Details) to specifically test whether diet could attenuate the effect of age on each metabolite. While a few weak associations were observed, no strong relations were found for any of these analyses (Figure 2A). However, we observed that the majority of significant changes in individual metabolites were attributed to DR alone (Figure 2A, blue dots), with far fewer metabolites affected by only age (Figure 2A, red dots) or by both diet and age (Figure 2A, green dots). We also asked whether the sign and strength of the effect of diet or of age on each of the metabolites measured in one tissue was associated with the effect in other tissues. We found that the effect of diet on metabolites, as measured by β values, was highly correlated across tissues. In contrast, the effect of age on metabolite levels appears to be highly tissue specific (Figure 2B). We also found that the effect of diet on metabolite levels in human serum and rat plasma was significantly and positively correlated ($p < 0.01$).

The Aging Rat Metabolome Is Defined by an Increase in Circulating Glycerophospholipids

Reductions in various amino acids, acylcarnitines, and other fatty acids were previously reported to define the aging mouse blood metabolome (Houtkooper et al., 2011); thus, we evaluated these metabolites in our experimental model. Principal-component analysis (PCA) in rat plasma illustrated that the metabolomic profiles for YAL and OAL are distinct. PC1, which separates YAL and OAL samples, is heavily influenced by changes in glycerophospholipids (Figure 3A). Indeed, we observed a generalized, significant increase in many glycerophospholipids; amino acids such as proline (Pro) ($p = 0.007$; false discovery rate [FDR] $\alpha = 0.05$), threonine (Thr) ($p = 1.35 \times 10^{-5}$), glycine (Gly) ($p = 0.028$), and alanine (Ala) ($p = 0.024$); the acylcarnitine C14:1 ($p < 0.001$); and approximately half of the detected sphingolipids in rat plasma with aging per se (Figure 3B; Table S1). A similar increase

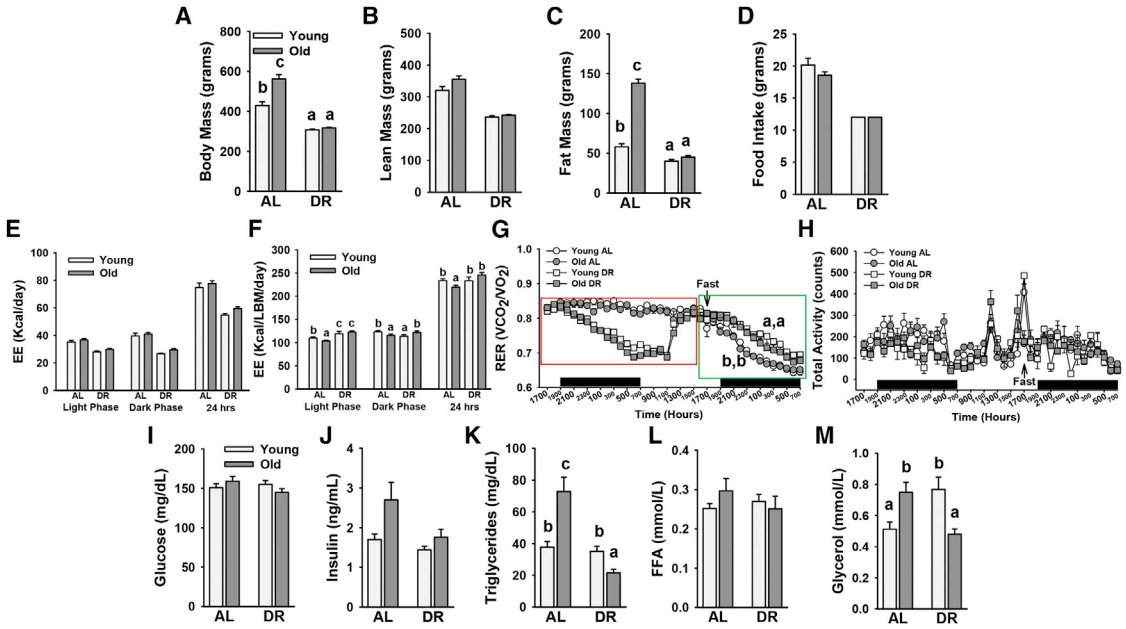

Figure 1. Phenotypic Characteristics of Young and Old AL-Fed and DR Rats

(A–D) Total body mass (A), but not LBM (B), were increased with aging, while fat mass was also increased with age (C), which was prevented by lifelong DR to ~60% of AL intake (D) (n = 8 per group).

(E and F) Energy expenditure tended to be reduced in young and old DR rats (E), but adjusting for LBM revealed a preservation in metabolic rate with DR (F) (n = 8 per group).

(G and H) Substrate utilization was measured during a 24-hr light and dark photoperiod, as well as in response to an overnight fast. As indicated in the red box, DR per se led to a lower RER, particularly during the dark photoperiod, a time in which DR mice are fasted, while RER did not vary with age in AL-fed groups (G). However, an overnight fast resulted in a more severe reduction in RER for AL animals than those on DR. Furthermore, no difference was observed in spontaneous activity among groups (H) (n = 8 per group).

(I–K) Fasting glucose levels (I) were similar among groups, but OAL animals tended to have elevated insulin levels (J) and significantly increased TG levels (K), which were prevented by lifelong DR (n = 8 per group).

(L and M) Plasma FFA levels did not vary among groups (L), but free glycerol was markedly elevated in YDR and OAL, respectively (M) (n = 8 per group). Glucose and insulin were measured in duplicate, and FFA, TG, and glycerol were assessed in triplicate. Bars and lines represent means ± SEMs. Different letters denote a significant difference between groups, $p \leq 0.05$.

in the sphingolipid SM.C16:1 (p = 0.0008), the acylcarnitine C16:1 (p = 0.05, but non-significant [NS] after FDR correction), and lysoPCaC16:0 (p = 0.039) were observed with age per se in humans, while lysoPCaC17:0 (p = 0.0016), lysoPCaC18:2 (p = 0.011; FDR α = 0.2), lysoPCaC20:3 (p = 0.0002; FDR α = 0.05), and lysoPCaC20:4 (p = 0.0014) were downregulated with age per se in human serum (Table S2).

Lifelong DR Opposes the Age-Related Increase in Several Plasma Metabolites

We next determined to what extent the observed shifts in metabolites were an inevitable consequence of aging or whether these alterations were modifiable by lifelong DR. While comparing the slopes of age and diet on all of the metabolites did not suggest a strong effect of DR on age (Figure 2A), PCA clearly demonstrates that YDR and ODR metabolomic profiles cluster together, irrespective of age (Figure 3A). DR opposed the age-related increase in nearly half of the detected glycerophospholipids and sphingolipids (interaction FDR α = 0.05 for the majority of metabolites) and a minority of amino acids (glutamine [Gln] [interaction p = 0.009; FDR α = 0.05] and arginine [Arg] [p = 0.02]) and acylcarnitines (C14:1 [p = 0.0009] and C3 [p = 0.0014]) (Figures 3C and 3D). In addition, a small metabolite screen by gas chromatography-mass spectrometry (GC-MS) determined that a minority of other metabolites found to increase in rat plasma with aging, including ribose 5-phosphate (interaction $p = 9.13 \times 10^{-6}$; FDR α = 0.05), dehydroepiandrosterone (interaction $p = 1.77 \times 10^{-5}$), and glycerolphosphate (interaction p = 0.0018), were maintained at youthful levels by lifelong DR (Table S1). However, DR did not significantly prevent age-related changes in 3-hydroxybutyric acid, pyrophosphate, or tetradecanoic acid.

In humans, only a limited number of effects were congruent with those found in rodents (Figure S1; Table S2). For instance, glutamic acid, which did not change with age in either species, was similarly reduced by DR in rodents (p = 0.0006; FDR α = 0.05) and humans (p = 0.0001; FDR α = 0.05). However, a number of other metabolites identified as changing in rodents, were either not altered in humans or presented with disparate results. While circulating glycerophospholipids were robustly and consistently elevated in OAL rat plasma, a more modest number of glycerophospholipids were affected by age in human serum (lysoPCaC17:0, lysoPCaC18:1, lysoPCaC18:2, lysoPCaC20:3, lysoPCaC20:4, lysoPCaC28:0, and lysoPCaC32:0), and these metabolites tended to be reduced rather than increased with

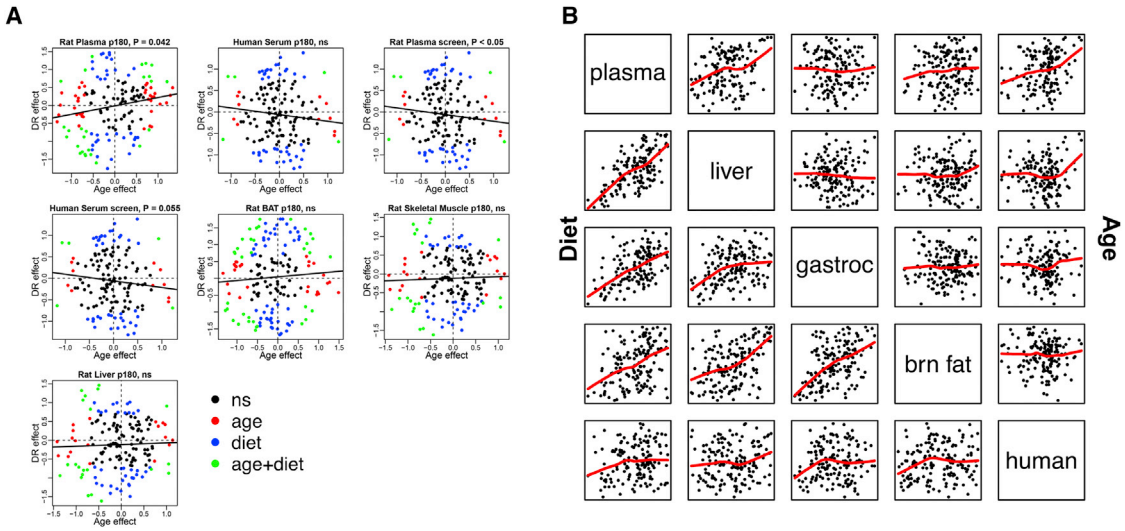

Figure 2. Impact of Aging versus Diet on the Metabolome in Rats and Humans

(A) x and y axes indicate the value of β for the effect of age and diet, respectively, on each metabolite, shown as individual points. The β values are taken from the linear model, $\hat{y}_i = \alpha + \beta_1 age + \beta_2 diet + \varepsilon$ (see Method Details), with statistical significance ($p \leq 0.05$) indicated by color. A negative correlation across metabolites suggests that the effect of DR on metabolite levels acts opposite to the effect of age on metabolite levels. Metabolites were detected via the Biocrates AbsoluteIDQ p180 and GC-MS small metabolite screen modules. The figures indicate a slight but significant negative correlation between age and diet effects for rat plasma and human serum (GC-MS screen), but not in rat tissues. Furthermore, we generally observed more significant effects on metabolite levels for DR alone (blue) versus age alone (red) or for both DR and age (green).

(B) Correlation plots between β values of individual metabolites across sample type for plasma, serum, and tissue analytes, as measured via the Biocrates AbsoluteIDQ p180 kit. Between-tissue comparisons are given for diet (lower diagonal) and age (upper diagonal). Strong correlations were observed among rat plasma and tissues for the effects of diet but not age. Likewise, a significant correlation was observed in the response to DR between human serum and rat plasma ($p < 0.01$).

age. Likewise, the acylcarnitine C14:1 was reduced with human aging (interaction $p = 0.001$; FDR $\alpha = 0.2$) and tended to be maintained by DR, while C14:1 levels in rodents increased with aging and were reduced by DR. Discrepant effects were also observed with DR per se between species. The longer-chain glycerophospholipids (PCaeC42:1, PCaeC42:2, and PCaeC42:3) tended to be increased in humans engaged in long-term DR, but the same metabolites in rodents were increased with age rather than with DR.

Some Age-Related Perturbations to the Rat BAT Metabolome Are Attenuated by DR

We next assessed the metabolome in rat BAT. Similar to plasma, PC1 demonstrates a very strong effect of diet on the BAT metabolome, clearly separating the AL and DR groups. As with plasma, there is a smaller effect of age in BAT, although the effect of age is more clearly visualized in AL versus DR groups (Figure S2A). In contrast to plasma, robust reductions were noted for some amino acids (citrulline [Cit], Gly, Gln, and histidine [His]) and several glycerophospholipids, sphingolipids, and biogenic amines, all of which characterized the age-related metabolomic footprint in this tissue, although very few acylcarnitines were affected ($p < 0.05$; Figure S2B; Table S3). DR robustly counteracted age-related changes in several BAT metabolites, particularly glycerophospholipids, and tended to preserve Cit and His levels (FDR $\alpha = 0.2$), but not other amino acids. DR per se also resulted in marked effects on some metabolites, which resembled changes observed with age per se, including elevated levels of PCaaC34:1, PCaa36:3, and SM.C24:0 and lower levels of spermidine (Figure S2; Table S3).

Diverse Changes in Rat SkM and Liver Metabolites with Aging and DR

In rat gastrocnemius muscle (SkM), PC3 revealed a strong effect of age on the metabolome, particularly glycerophospholipids and lysine (Lys), Arg, carnosine, and C4, but DR attenuated much of the age effect on the metabolomic profile in this tissue (Figure S3A). A significant effect of age was observed for several amino acids analyzed, including Arg, asparagine (Asn), His, Lys, ornithine (Orn), Pro, and serine (Ser) (FDR $\alpha = 0.05$), as were the biogenic amines carnosine ($p = 0.001$), kynurenine ($p = 0.007$), and sarcosine ($p = 0.014$) (Figure S3B; Table S4). Several glycerophospholipids were also perturbed in aged SkM, with some metabolites, including lysoPCaC16:0 ($p = 0.001$; FDR $\alpha = 0.05$) and PCaaC34.3 ($p = 0.014$), generally increased with age. However, several longer, more unsaturated glycerophospholipids, including PCaaC36:5 ($p = 0.005$), PCaaC36:6 ($p = 0.001$), PCaaC38:6 ($p = 1.82 \times 10^{-6}$), and PCaaC40:6 ($p = 3.7 \times 10^{-7}$) were reduced with age. In contrast, age-related changes in some acylcarnitines were characterized by an increase in metabolites (C14, C16, C18:2), while several shorter acylcarnitines, including C3 ($p = 0.028$; FDR $\alpha = 0.2$), C4 ($p = 0.001$), and C5 ($p = 0.001$), were decreased. Lifelong DR protected against some of the perturbations to amino acids, including Arg and Lys, and the biogenic amine carnosine (Table S2). Similar to BAT, DR attenuated age-related changes in SkM for some glycerophospholipids altered

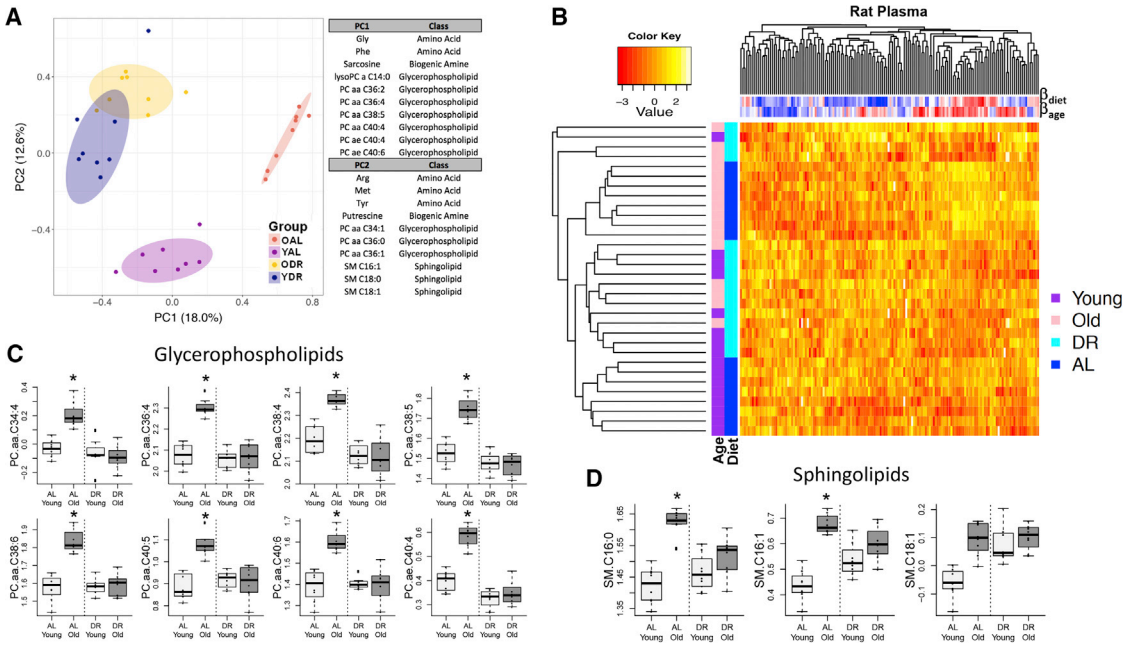

Figure 3. Biocrates Metabolomic Analysis in Rat Plasma with Aging and DR

(A) PC1 metabolites reveal that while shifts in the plasma metabolome can be discriminated by age, metabolites cluster in similar quadrants with DR, regardless of age. These features of age and diet were largely driven by glycerophosholipids and to a lesser extent by amino acids and sphingolipids.

(B) Heatmap of all metabolites analyzed illustrating hierarchical clustering of plasma levels with age and diet.

(C) Representative glycerophospholipid metabolites in which a significant age × diet interaction was observed. Post hoc comparisons for these metabolites detected an increase in levels for OAL rats, which were completely attenuated by lifelong DR (n = 8 per group).

(D) Representative sphingolipids in which an age × diet interaction was observed. Post hoc comparisons detected an age-related increase in the levels of these metabolites, but DR only opposed the increase in SM.C16:0 and SM.C16:1, while DR led to a similar increase in SM.C18:1 levels as age (n = 8 per group). Samples were measured by single detection, and no coefficient of variation (CV) was calculated for this dataset because a low number of technical replicates (2) were included in the run. See Table S7 for CVs of the same individual metabolites with the Biocrates assay from 6 technical replicates in a separate run on FBN plasma samples.

Box and whisker plots represent lower and upper quartile ranges and highest and lowest observations, respectively, and heavy black lines indicate the median. Dot plots overlaid on boxes represent individual data points. The asterisk indicates significantly different from other experimental groups, $p \leq 0.05$.

by age, while the effect of DR closely resembled the effect of age on other metabolite levels, such as PCaaC38:0, PCaaC40:6, and PCaeC40:6 (Figures S3C and S3D).

In liver, the metabolites that make up PC2, which were almost entirely glycerophospholipids, revealed a strong effect of age on the metabolome, although a diet × age interaction was evident due to the high overlap of DR groups on the PCA plot, irrespective of age (Figure S4A). A small minority of amino acids (Cit, Thr, isoleucine [Ile], valine [Val], phenylalanine [Phe], and Pro) were affected by age per se in the liver, and these changes were largely unaffected by DR (Figure S4B; Table S5). Meanwhile, the effect of aging on other lipids was more complex, with glycerophospholipids either significantly increased or decreased, respectively, while nearly 60% of measured sphingolipids were increased with age. DR failed to counteract age-related changes in liver sphingolipids but was able to attenuate changes in several glycerophospholipids (Figures S4C and S4D; Table S5).

Circulating Sarcosine Is Similarly Modulated by Aging and DR in Rodents and Humans

We next examined the rat and human metabolome for metabolites demonstrating conserved changes with aging and diet. Among nearly 400 detected metabolites, only sarcosine was found to be similarly altered with aging and DR, as determined by the Biocrates AbsoluteIDQ p180 kit. Specifically, sarcosine was reduced in circulation with aging per se in rats ($p = 0.0002$; FDR $\alpha = 0.05$) and humans ($p = 0.0056$; FDR $\alpha = 0.15$), while DR per se increased levels in rats ($p = 0.0001$; FDR $\alpha = 0.05$) and humans ($p = 0.0059$; FDR $\alpha = 0.08$). Furthermore, DR prevented the age-related decline in rat plasma sarcosine, maintaining levels comparable to young animals (interaction $p = 0.021$) (Figures 4A and 4B). We further observed that both young and old Ames dwarf mice had markedly elevated levels of sarcosine in serum (Figure 4C), a finding that is in agreement with the enhanced liver GNMT activity previously documented in these mice (Uthus and Brown-Borg, 2003). Metscape analysis of metabolite networks confirmed that sarcosine is integral to metabolite shifts with aging and DR in rats and humans (Figures 4D–4G). In liver, sarcosine levels were relatively unchanged with aging, but were reduced by DR (Figure 4H). Meanwhile, GNMT, which is the most abundant methyltransferase in liver and thought to be a major source of circulating sarcosine, via the conversion of *S*-adenosyl Met (SAM) and glycine to *S*-adenosyl homocysteine (SAH) and sarcosine, demonstrated reduced

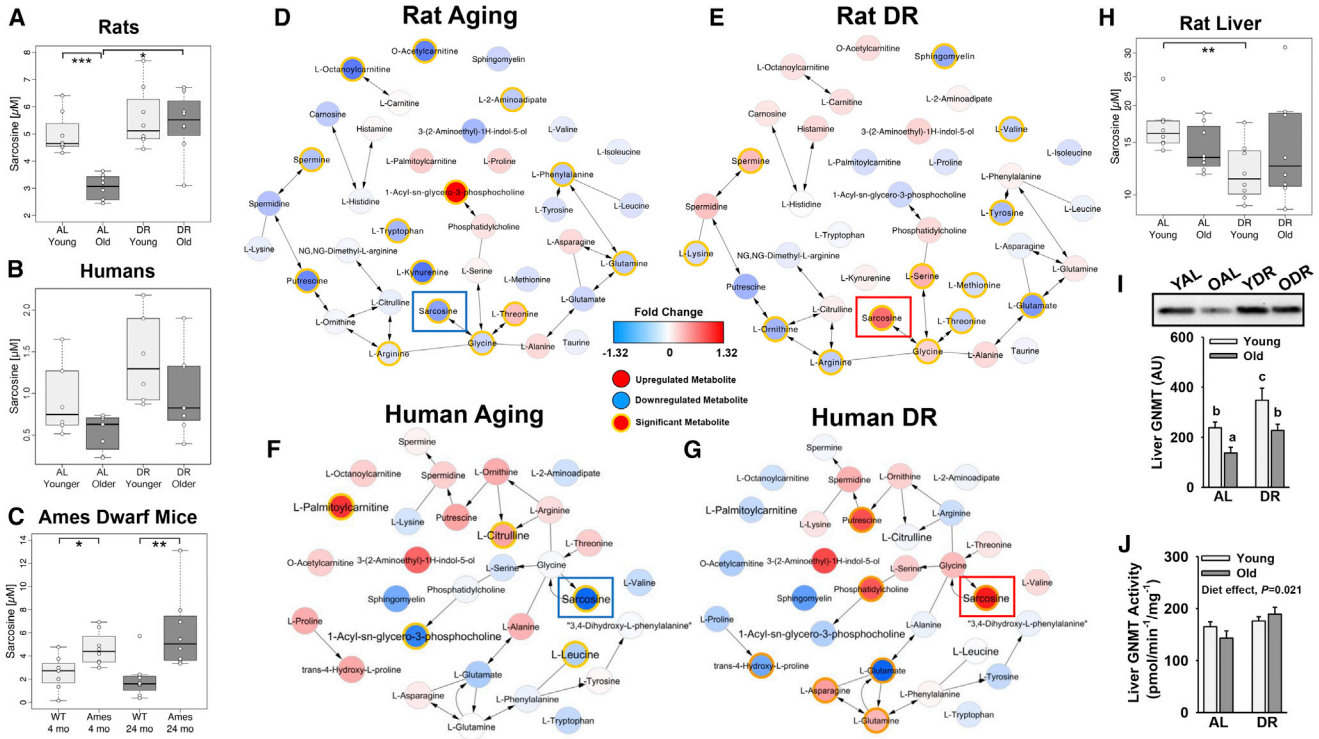

Figure 4. Sarcosine Is Uniquely Modulated and Integral to the Aging and DR Effects on the Rat and the Human Metabolome

(A and B) Among all of the detected metabolites, only sarcosine levels were similarly reduced with aging and increased by DR in rats (A) and humans (B) (n = 8 per group for rats; n = 6–7 per group for humans).

(C) Sarcosine is significantly elevated in young and old long-lived Ames dwarf mice (n = 8 per group).

(D–G) Metscape analysis identifies sarcosine as similarly modulated within the metabolite network by aging (blue circle; downregulated) and DR (red circle; upregulated) in rats (D and E) and humans (F and G).

(H–J) Liver sarcosine is reduced with DR, but not with age (H). Meanwhile, liver GNMT expression decreases with age but is increased by DR (I), while GNMT activity was numerically decreased with aging and increased by DR (J) (age $p = 0.276$, diet $p = 0.039$, age × diet $p = 0.232$).

Box and whisker plots represent lower and upper quartile ranges and highest and lowest observations, respectively, and heavy black lines indicate the median. Dot plots overlaid on boxes represent individual data points. Metabolomic detection of sarcosine and liver GNMT levels were measured by single detection, and GNMT activity was measured in duplicate. Bars represent means ± SEMs, n = 8 per group. Brackets with asterisks indicate a significant difference between groups: *$p \leq 0.05$, **$p < 0.01$, ***$p < 0.001$. Different letters denote a significant difference between groups, $p \leq 0.05$.

expression with aging. Meanwhile, GNMT content (Figure 4I; $p < 0.05$) and activity were increased by DR per se (Figure 4J; age $p = 0.396$, diet $p = 0.021$, interaction $p = 0.147$).

Sarcosine Replacement in Old Animals Alters the Plasma Metabolome

Next, we aimed to determine whether restoring sarcosine to more youthful levels could alter the aging metabolome and recapitulate at least some of the DR effects on plasma metabolites. Old FBN rats were provided either regular chow (control) or a matched diet supplemented with sarcosine (1,250 mg/kg) for 8 weeks (n = 8 per group). A metabolomic analysis confirmed that plasma sarcosine was increased nearly 60% by the diet (Figure 5A; $p < 0.05$). However, no effect was observed on body weight, composition, food intake, and glucose or insulin levels in old sarcosine-replete rats (Figures 5B–5F). However, PCA revealed that the metabolome from old sarcosine-fed rats was distinct from controls (Figure 5G) and that global differences were well visualized by heat cluster map (Figure S5A), with a shift in a minority of metabolites, including Glu, Trp, Met-sulfoxide (Met-SO), and several glycerophospholipids, although these effects were no longer significant after adjusting for the FDR. Furthermore, using correlations between metabolites to construct a sarcosine network, a high "betweenness" score was identified for sarcosine in the linkage of amines, amino acids, and lipids (Figures 5H and S5B). Glutamate was most strongly correlated with sarcosine ($p < 0.001$; Figures 5H, S5B, and S5C), while sarcosine was also significantly and positively correlated with the polyamines spermidine ($p = 0.034$) and spermine ($p = 0.034$) (FDR $\alpha = 0.12$; Figures S5B and S5C).

To more specifically examine the relation of sarcosine and age, as well as the impact of sarcosine replacement on one-carbon metabolism in old animals, we performed a second refeeding experiment in aged FBN rats for 4 weeks. Using a fluorescent-based sarcosine assay in young (4 mo; n = 8), middle-aged (12 mo; n = 8), old (25–26 mo; n = 10), and old sarcosine-supplemented male FBN rats (n = 10), we confirmed that plasma sarcosine was similar between young and middle-aged animals but

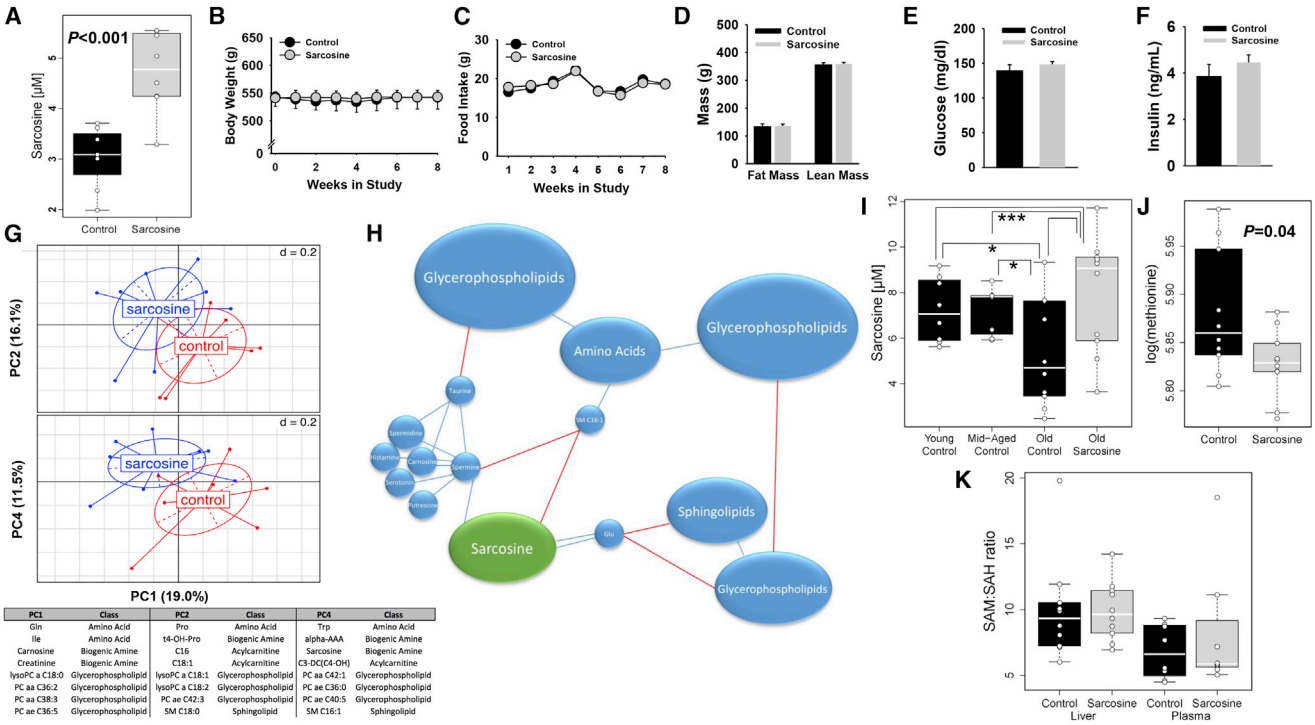

PC1	Class	PC2	Class	PC4	Class
Gln	Amino Acid	Pro	Amino Acid	Trp	Amino Acid
Ile	Amino Acid	t4-OH-Pro	Biogenic Amine	alpha-AAA	Biogenic Amine
Carnosine	Biogenic Amine	C16	Acylcarnitine	Sarcosine	Biogenic Amine
Creatinine	Biogenic Amine	C18:1	Acylcarnitine	C3-DC(C4-OH)	Acylcarnitine
lysoPC a C18:0	Glycerophospholipid	lysoPC a C18:1	Glycerophospholipid	PC aa C42:1	Glycerophospholipid
PC aa C36:2	Glycerophospholipid	lysoPC a C18:2	Glycerophospholipid	PC ae C36:0	Glycerophospholipid
PC aa C38:3	Glycerophospholipid	PC ae C42:3	Glycerophospholipid	PC ae C40:5	Glycerophospholipid
PC ae C36:5	Glycerophospholipid	SM C18:0	Sphingolipid	SM C16:1	Sphingolipid

Figure 5. Sarcosine Refeeding Alters the Old Rat Metabolome and Is an Integral Node Linking Diverse Plasma Metabolites

(A) Sarcosine feeding in aged rats for 8 weeks was able to raise plasma sarcosine levels (n = 8 per group).

(B–F) Sarcosine-fed rats had no significant change in body weight (B), food intake (C), fat mass, lean mass (D), glucose (E), or insulin levels (F) (n = 8 per group).

(G) Despite no effect on gross phenotypic characteristics, PCA confirmed that 8 weeks of sarcosine supplementation in old rats (red) resulted in distinct clustering of metabolites, as compared to controls (blue), which can be further visualized by heat cluster map (see Figure S5A).

(H) Representative simplified correlation map of sarcosine levels with other metabolites. See Figure S5B for the corresponding detailed correlation map. Sarcosine is shown in green, and other metabolites/nodes are shown in blue. The size of the nodes is representative of the number of correlated metabolites at a given node. Blue interconnecting lines indicate a positive correlation, and red lines indicate a negative correlation. Double lines indicate that a strong correlation exists between metabolites, as was found with glutamate ($p < 0.001$). Sarcosine was also positively related to spermine and spermidine (see Figure S5C) and demonstrated a high "betweenness" score among metabolites.

(I–K) Examination of sarcosine levels across multiple ages confirms that levels do not decline until older age. Furthermore, 4 weeks of sarcosine feeding raised sarcosine levels in old animals (I), and correspondingly reduced Met levels (J), without effects on the plasma or liver SAM:SAH ratio (K) (n = 8–10 per group). Sarcosine, liver GNMT levels, and plasma SAM and SAH were measured by single detection, while GNMT activity and liver SAM and SAH were measured in duplicate.

Box and whisker plots represent the lower and upper quartile ranges and highest and lowest observations, respectively, and heavy white lines indicate the median. Bars and lines represent means ± SEMs. Dot plots overlaid on boxes represent individual data points. Unless otherwise stated, brackets with asterisks indicate a significant difference between groups: *$p \leq 0.05$, ***$p < 0.001$.

significantly decreased at 25 mo, and this age-related reduction was restored by sarcosine feeding (Figure 5I; $p < 0.05$). We next performed targeted metabolomics in plasma from old control (n = 10) and old sarcosine-supplemented rats (n = 10) for intermediates involved in folate, Met, glycine, and sarcosine metabolism. We observed that sarcosine led to a significant reduction in plasma Met levels (Figure 5J; $p = 0.04$), but it did not alter the SAM:SAH ratio in plasma or liver (Figure 5K). Sarcosine feeding did tend to increase plasma glycine ($p = 0.10$) and *N*-acetyl glycine levels ($p = 0.06$; Figure S6A), but no effects were observed on other related plasma metabolites, such as choline, serine, betaine, or dimethylglycine (Figure S6A).

To better understand to what extent sarcosine levels are dynamically regulated, including circadian effects and nutrient availability, we collected serial blood samples from an indwelling catheter at 4-hr intervals throughout the day in young rats. As can be observed in Figure S6B, plasma sarcosine levels were relatively unchanged on average in a 12-hr period, although some variability was observed across time points in individual animals (Figure S6C). Furthermore, when samples were collected under fasted and refed conditions, respectively, there was no significant effect of nutrient status on sarcosine concentrations (Figures S6D and S6E). Thus, these data suggest that the ability of DR to maintain "youthful" sarcosine levels in old animals is likely adaptive rather than dynamically regulated by nutrient availability per se.

Sarcosine Stimulates Autophagic Flux *In Vitro* and *In Vivo*

To determine whether elevated sarcosine may serve as more than simply a biomarker of aging and DR, we next investigated whether sarcosine may have direct effects on cellular processes

implicated in aging. Given the tight connection between metabolism and proteostasis, including the reported inhibitory effect of SAM levels on autophagy (Sutter et al., 2013), we decided to determine whether sarcosine could serve to activate autophagy. We first used NIH 3T3 mouse fibroblasts and two different fluorescent reporters to quantify the activity of the two types of mammalian autophagy known to decline with age—macroautophagy (mcherry-GFP-LC3) and chaperone-mediated autophagy (CMA, KFERQ-PS-Dendra2) (Kimura et al., 2007; Koga et al., 2011b). The mCherry-GFP-LC3 reporter is used to label autophagosomes. As they fuse with lysosomes, GFP fluorescence is quenched due to the low lysosomal pH resulting in mCherry-only labeled autolysosomes. Sarcosine stimulated basal macroautophagy in a dose-dependent manner and to a lesser extent macroautophagy induced by serum removal (Figures 6A and 6B). A separate analysis of changes in the different vesicular compartments involved in autophagy revealed that sarcosine enhanced macroautophagy induction (quantified by autophagic vesicle number) as well as increased efficiency of lysosomal clearance of autophagosomes, as shown by an increased number of autolysosomes without a concomitant increase in autophagosomes (Figures 6C–6E). Analysis of autophagic flux by quantification of the degradation of the well-established autophagic cargo p62 also confirmed a dose-dependent increase in p62 clearance in cells treated with sarcosine (Figure 6F). The effect of sarcosine seems to be selective on macroautophagy rather than a general improvement of all lysosomal pathways, since analysis of a second form of autophagy, CMA, in the same cells did not reveal significant changes in basal CMA or CMA induced by serum deprivation or oxidative stress following increasing concentrations of sarcosine (Figures S7A–S7D). Induction of autophagy by sarcosine was more discrete than was observed by known inducers such as rapamycin and spermidine, but it was more effective than metformin (Figure 6G; $p < 0.05$). Sarcosine (500 μM) showed partially additive effects on induction of macroautophagy by serum removal and oxidative stress, suggesting alternative mechanisms of autophagic activation through sarcosine, compared to these stressors (Figure 6H). However, sarcosine had no additional effect upon macroautophagy activation through endoplasmic reticulum (ER) stress or lipid stimuli.

Although identification of the mechanism by which sarcosine stimulates autophagy is beyond the scope of the present study, considering the close connections between nutrition and autophagy and the key role that the mechanistic target of rapamycin (mTOR) plays in both processes, we next analyzed the status of mTOR signaling (Figures 6I and 6J). In treated cells, we found a trend toward increased mTOR phosphorylation and TOR complex 1 (TORC1) signaling (using pS6 as a readout), without noticeable changes in TORC2 (pAktSer473 levels). TORC1 is a well-established macroautophagy inhibitor during nutrient sufficiency, in part through direct phosphorylation of the autophagy effector Ulk1 at Ser 757, thus preventing its interaction with the activating kinase 5′ adenosine monophosphate-activated protein kinase (AMPK) (Kim et al., 2011). Despite higher TORC1 activity, sarcosine-treated cells displayed significantly higher phosphorylation of Ulk at Ser 555, one of the AMPK sites (Figures 6I and 6J). These results suggest that sarcosine is able to stimulate macroautophagy over a background of enhanced mTOR signaling, likely by potentiating the stimulatory effect of AMPK on macroautophagy.

Finally, we determined whether sarcosine can activate *in vivo* autophagy in the liver of old rats fed a standard chow diet or a sarcosine-supplemented diet for 10 days. Sarcosine-treated animals displayed lower levels of the autophagic cargo p62 and showed increased autophagic flux (measured as both clearance of LC3-II and p62) in the liver (Figure 7A). Furthermore, electron microscopy and morphometric analysis revealed similar numbers of autophagic vacuoles in the livers from both groups of rats but a significantly higher abundance of autolysosomes and reduced autophagosome content in sarcosine-supplemented animals (Figures 7B and S7E). In fact, autophagosomes containing high-density lipofuscin pigment (indicative of poor degradation) were highly abundant in the control group but rarely observed in the sarcosine-fed animals (Figure S7E), while the percentage of vacuoles that matured into autolysosomes increased from <30% to >70% after only 10 days of sarcosine supplementation (Figure 7B). Thus, induction of macroautophagy by sarcosine also occurs *in vivo* and does not seem restricted to a specific cell type. Supporting that the beneficial effect of sarcosine treatment was coming to a large extent through serum, incubation of 3T3 cells with heat-inactivated serum from old sarcosine-treated rats led to less inhibition of autophagy, as compared to old control rat serum (Figure 7C). Moreover, while sarcosine levels per se do not appear to demonstrate a discernible diurnal pattern, the ability of sarcosine to activate autophagy was highly dependent on time of day, because less inhibitory effects were limited to samples obtained at 9 a.m. and not at later time points taken throughout the day (Figure S7F). Furthermore, sarcosine treatment tended to activate a similar signaling network in liver, as observed in 3T3 cells, evidenced by a strong induction in pS6 and numerical increase in phospho-AMPK (pAMPK) (Figures 7D and 7E).

DISCUSSION

Investigations into the metabolism-aging interplay focusing on changes at the level of the metabolome have been increasingly reported in a variety of model organisms (Hoffman et al., 2016; Laye et al., 2015; Lewis et al., 2018; Ma et al., 2015; Pontoizeau et al., 2014). Studies have also been conducted in humans, including one report linking several lipid species to human longevity (Gonzalez-Covarrubias et al., 2013) and another noting associations among citric acid cycle intermediates and bile acids on the lifespan in humans (Cheng et al., 2015). However, arriving at consensus changes that define the aging metabolome has proven somewhat elusive, given the inherent complexity of the metabolome, as well as other variables across studies (De Guzman et al., 2013; Hoffman et al., 2016; Kim et al., 2014; Ma et al., 2015). Furthermore, to what extent changes to the aging metabolome are amenable to interventions such as DR, and more important, the human relevance of these observations, is not well understood. Here, we attempted to address some of these issues using both rodent and human cohorts of aging and DR. We show that shifts in circulating and tissue glycerophospholipids, as well as other lipids and amino acids, define

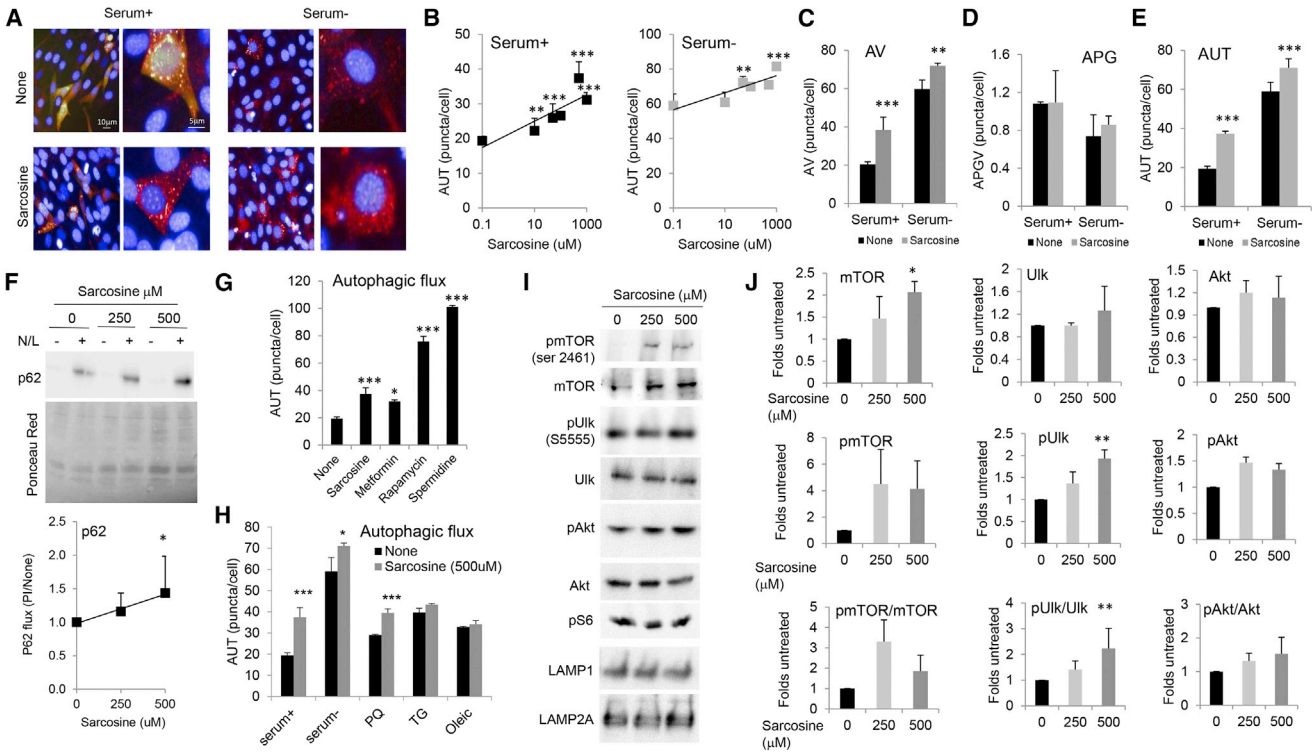

Figure 6. Effect of Sarcosine on Macroautophagy *In Vitro*

(A) Mouse fibroblasts in culture (NIH 3T3 cells) expressing the tandem reporter mCherry-GFP-LC3 were exposed to the indicated concentrations of sarcosine for 16 hr in the absence or presence of other autophagy inducers. Representative images of both controls and cells treated with 500 μM sarcosine in the presence or absence of serum are shown.

(B) Quantification of autophagic flux (number of autophagosomes matured into autolysosomes) at the indicated sarcosine concentrations shows a dose response to sarcosine (n > 2,500 cells).

(C–E) Number of autophagic vacuoles (AVs; C), autophagosomes (APGs; D) and autolysosomes (AUTs; E) in cells treated with sarcosine (500 μM) show increased induction (vesicle count) and efficient clearance (AUT/APGs) of APGs (n > 2,500 cells).

(F) Degradation of the autophagic cargo p62 in cells treated with increasing concentrations of sarcosine. Top: representative immunoblot. Bottom: quantification of the changes in p62 upon addition of lysosomal inhibitors ammonium chloride and leupeptin ammonium chloride and leupeptin (N/L) (n > 4 cells per condition).

(G) A comparative analysis of several well-known inducers of autophagy with sarcosine. Sarcosine is more effective than metformin at inducing autophagy but less effective than rapamycin and spermidine (n > 2,500 cells). Quantification was done using high-content microscopy. Differences with untreated ("none") are indicated.

(H) Effect of the indicated treatments alone or in combination with 500 μM sarcosine on autophagic flux in cultured mouse fibroblasts. Several methods of autophagic induction were investigated, including oxidative damage (paraquat [PQ]), ER stress (thapsigargin [TG]) and lipotoxicity (oleic) in addition to serum-starved induction. Sarcosine showed an additive effect to serum starvation and paraquat, suggesting alternate mechanisms of activation, but not to thapsigargin or lipotoxicity (n > 2,500 cells).

(I and J) Representative immunoblots (I) and densitometry analysis (J) in 3T3 cells demonstrate that sarcosine activates the mTOR signaling pathway in cells, but that this occurs in concert with Ulk and LAMP1 activation, suggesting that AMPK activity is also increased, thereby permitting increased autophagy in spite of mTOR activation.

All results were obtained from a minimum of 3 independent experiments unless otherwise stated. Bars and lines indicate means ± SEMs (n = 3–4 per treatment). Significantly different from control: *p < 0.05, **p < 0.01, and ***p < 0.001.

the aging rat plasma metabolome, although the directionality of some changes were distinct from prior reports (Houtkooper et al., 2011). Furthermore, we found that DR is a stronger driver of the metabolome than is age, based upon PCA in rat plasma and tissues. Most important, we identified that the biogenic amine sarcosine, as similarly modulated by aging and DR in rodents and humans. Moreover, this metabolite is markedly elevated in dwarf mice and is capable of stimulating macroautophagy *in vitro* and *in vivo*.

The growth hormone/insulin-like growth factor-1 (GH/IGF-1) and mTOR signaling pathways play an integral role in the beneficial effects of DR on aging and longevity (Barzilai et al., 2012; Fontana et al., 2010b). In addition to a reduction in calories, evidence has also implicated Met restriction as an important mediator of the DR effect (Orentreich et al., 1993; Richie et al., 1994), and Met interacts with the GH/IGF-1 pathway to extend lifespan in mice (Brown-Borg et al., 2014). Furthermore, Met is an essential precursor to SAM, and the conversion of SAM to SAH by GNMT produces sarcosine (Obata and Miura, 2015). GNMT is the most abundant methyltransferase in liver and is upregulated in Ames dwarf mice (Uthus and Brown-Borg, 2003), while GH replacement can suppress GNMT activity (Aida et al., 1997;

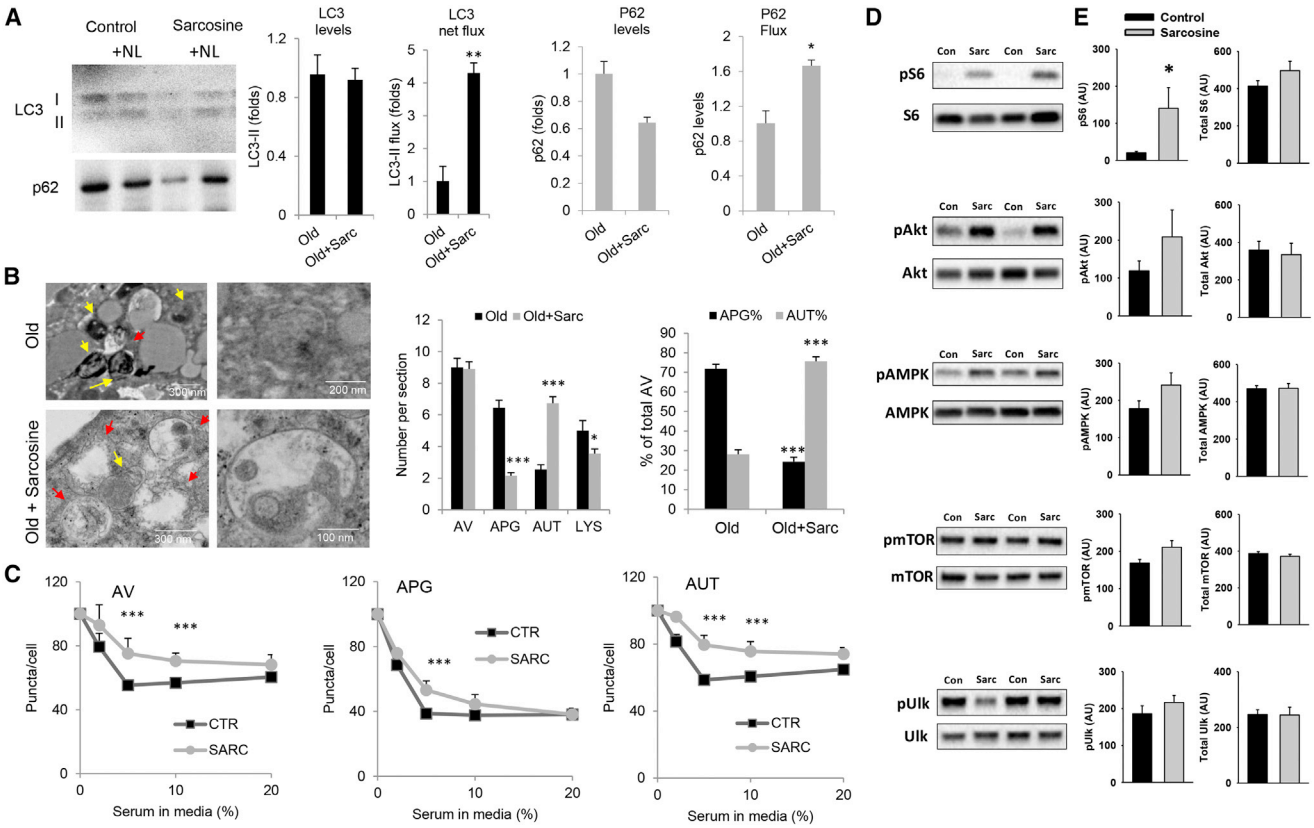

Figure 7. Effect of Sarcosine on Macroautophagy *In Vivo*

(A) Autophagic flux increases in rat liver after short-term (10 days) dietary sarcosine feeding. Treatment with the inhibitors of lysosomal proteolysis (20 mM ammonium chloride and 100 μm leupeptin; N/L) revealed that degradation of LC3 and p62 in lysosomes was accelerated in the sarcosine-treated group. Representative immunoblot (left) and quantification of the levels and flux of LC3 and p62 (right) are both shown. n = 3 per group.

(B) Effect of a short-term (10 days) dietary sarcosine treatment on the autophagic compartments in aged rat liver. Low-magnification images (left) and examples of the autophagic compartments more abundant in each of the groups (APGs in untreated and autolysosomes [AUTs] in sarcosine treated). Red arrows indicate AUTs, and yellow arrows indicate APGs. Quantification of the number of AVs, APGs, AUTs and lysosomes (LYSs) per section (left) and the percentage of AVs that display characteristics of APGs or AUTs (right) are shown. Data reveal improved maturation of APGs into AUTs after sarcosine treatment, which is indicative of increased autophagic flux (n = 20 sections from 3 different animals). More examples of each compartment are shown in Figure S7E.

(C) Effect of old control and sarcosine-treated rat serum on autophagy. Heat-inactivated serum collected from old control or sarcosine-treated rats at 9 a.m. was added to the culture media of NIH 3T3 cells stably expressing the autophagy reporter mCherry-GFP-LC3. Cells were imaged, and the number per cell of AVs ($mCherry^+$ vesicles), APGs ($mCherry^+$ and GFP^+ vesicles), and AUTs (ALs, $mCherry^+$ GFP^- vesicles) were quantified using high-content microscopy (n > 2,500 cells). Differences with controls (supplemented with serum from untreated rats) were significant at most serum concentrations tested.

(D and E) Evaluation of signaling pathway activation in old rat liver following a short-term (10 days) dietary sarcosine treatment, as demonstrated by representative western blots (D) and the corresponding densitometry measurements (E), revealed that sarcosine increased pS6 *in vivo*, while a tendency toward increased activation of Akt and AMPK was observed (n = 8 per group).

All results were obtained from a minimum of 3 independent experiments unless otherwise stated. Lines and bars indicate means ± SEMs. Significantly different from controls: *p < 0.05, **p < 0.01, and ***p < 0.001.

Brown-Borg et al., 2005). Overexpression of GNMT increased lifespan in *D. melanogaster* (Obata and Miura, 2015), while knock down of GNMT resulted in reduced levels of sarcosine and abrogated the ability of DR to extend lifespan (Obata and Miura, 2015). These studies serve to illustrate the integral nature of the Met pathway, including modulation of Met, SAM, SAH, and sarcosine by GNMT in longevity. In agreement with this, our results show that DR per se preserves circulating sarcosine levels during aging and boosts liver GNMT expression and activity. It is important to note that while liver was used here as a surrogate tissue due to its high concentration of sarcosine-producing enzymes, GNMT is also expressed elsewhere, albeit at lower levels (Luka et al., 2009); thus, the relative contribution of liver versus other tissues as the source of circulating sarcosine with aging and diet perturbations will require further study. In addition, the markedly elevated sarcosine levels found in dwarf mice suggest that sarcosine may be an important component of the longevity phenotype in this model and across nature. The latter observation is in agreement with recent studies, not only in *D. melanogaster* (Obata and Miura, 2015) but also in aged mice (Kim et al., 2014).

Several recent studies have investigated the relation between sarcosine and a variety of diseases and disorders in humans with conflicting results. Elevated sarcosine levels in urine (Sreekumar et al., 2009) and serum (Koutros et al., 2013) have been

associated with prostate cancer progression, although this relation has not been observed in other reports (de Vogel et al., 2014; Jentzmik et al., 2011). Elevated urine sarcosine levels were also associated with incident type 2 diabetes (Svingen et al., 2016), while low levels of sarcosine in blood have been linked with advanced arteriosclerosis (Hasokawa et al., 2012) and several neurological disorders, including neuropathic pain (Barthel et al., 2014), cerebral ischemia (Pinto et al., 2014), seizure (Socała et al., 2010), and Parkinson disease (Tsai et al., 2014). More recently, serum sarcosine was shown to be increased by a 10-week aerobic exercise training program in previously untrained male subjects (Felder et al., 2017).

While sarcosine has been associated with various diseases and disorders, it is less clear whether sarcosine per se is a cause or simply a consequence in these instances. In support of the former possibility, sarcosine supplementation in humans has produced promising results as a primary therapy for Parkinson's disease with dementia (Tsai et al., 2014) and as an adjuvant treatment for patients suffering from schizophrenia (Strzelecki et al., 2015; Tsai et al., 2004). Likewise, beneficial effects of sarcosine have been found for learning and memory deficits (Kumar et al., 2016) and depression in rats (Chen et al., 2017). While sarcosine feeding in this study did not alter energy balance or endocrine status in aged rats, it did lead to discrete changes in the rat metabolome, including a reduction in plasma Met and a tendency toward boosting glycine pools. Sarcosine was also positively correlated with glutamate as well as spermidine and spermine, and SAM is involved in the biosynthesis of these polyamines. However, because no effect on the SAM:SAH ratio was detected, it is not entirely clear whether the reduction in Met by sarcosine feeding was in fact due to alterations in SAM metabolism or less homocysteine being recycled back to Met. However, the lack of changes in cysteine, betaine, and dimethylglycine levels does not support the latter possibility.

In addition to our identification of sarcosine as a biomarker of aging and DR, our data also demonstrate that this metabolite can impinge on pathways that are critical to proteostasis and directly modulate macroautophagy *in vitro* and *in vivo*. Autophagy and proteostasis decline with aging in several tissues (Kaushik and Cuervo, 2015; Madeo et al., 2015; Schneider et al., 2015) and can be modulated by related metabolites such as Met and SAM (Ruckenstuhl et al., 2014; Zubiete-Franco et al., 2016), which have been shown to inhibit autophagy (Sutter et al., 2013). We observed that sarcosine can directly stimulate basal macroautophagy in a dose-dependent manner *in vitro* and that this effect was recapitulated *in vivo* by sarcosine feeding, as demonstrated by an increase in autophagic flux and the clearance of autophagosomes and autophagic-like structures filled with lipofuscin-like dense material that accumulates in aged livers. Although a complete dissection of the mechanism behind sarcosine-induced autophagy requires further investigation, it was of interest that mTOR signaling and the AMPK pathway were both increased in response to sarcosine feeding. These findings suggest that sarcosine may be able to sustain enhanced autophagic flux in the context of mTOR activation by acting on AMPK, a well-known enhancer of autophagy. This activation of macroautophagy could contribute to improve proteostasis and increase resistance to stress, as previously described in DR. Ultimately, whether sarcosine supplementation can be harnessed to target some of the deleterious manifestations of aging through stimulation of autophagy is an intriguing possibility to explore in future studies.

Beyond sarcosine, another important observation was the overall increase in glycerophospholipids and sphingolipids in rat plasma with aging, although changes in glycerophospholipid levels among examined tissues were more complex. Studies have shown that increased incorporation of unsaturated phospholipids in the membrane lipid bilayer increases with age and that long-lived species have correspondingly lower levels of unsaturated fatty acids and a lower peroxidation index than their shorter-lived counterparts (Jové et al., 2013). However, DR prevented the age-related increase of several glycerophospholipids and sphingolipids in rat plasma, and to a lesser extent, changes to glycerophospholipids in BAT, SkM, and liver, respectively. In addition, lower concentrations of sphingolipids have been linked to healthy aging, because high levels found in plasma have been associated with disease, senescence, and reduced physical function (Trayssac et al., 2018; Wennberg et al., 2018). Consistent with this observation, our data show that several sphingolipids in plasma and tissue increased with aging in rodents and were substantially opposed by DR, although little effect of diet or age was observed in humans. Furthermore, conserved changes in metabolites with diet or age in humans were only detected for a minority of metabolites, while serum glycerophospholipids tended to decline rather than increase with age, as was the case in rodents. Thus, there is a clear heterogeneity that exists in the metabolomic response to diet and aging across species, strain, and, likely, sex that will need to be accounted for in future efforts (Jové et al., 2016).

In summary, using a rat model of aging, we have shown that DR is a robust modulator of the metabolome in plasma and tissues and effectively opposes a significant number of age-related changes in amino acids, glycerophospholipids, acylcarnitines, and sphingolipids in plasma and tissue. We have identified circulating sarcosine as a metabolite that is similarly and uniquely modulated by aging and DR in rats and humans and is dramatically elevated in the serum of long-lived Ames dwarf mice. Furthermore, supplementation studies in old animals identified sarcosine as a critical node linking amino acid and lipid metabolism, while mechanistic studies demonstrate sarcosine as a potent stimulator of basal macroautophagy, implicating an interesting link among aging, growth factors, metabolism, and proteostasis. Thus, these data identify sarcosine, which sits at the nexus of folate, Met, and glycine metabolism, as a potential functional biomarker of the aging and DR metabolic phenotype.

STAR★METHODS

Detailed methods are provided in the online version of this paper and include the following:

- KEY RESOURCES TABLE
- CONTACT FOR REAGENT AND RESOURCE SHARING
- EXPERIMENTAL MODEL AND SUBJECT DETAILS
- METHOD DETAILS
  - Basic physiology characteristics
  - Indirect calorimetry

SUPPLEMENTAL INFORMATION

Supplemental Information includes seven figures and seven tables and can be found with this article online at https://doi.org/10.1016/j.celrep.2018.09.065.

ACKNOWLEDGMENTS

This work has been supported by the National Institute on Aging (NIA) (R00AG037574 and R56AG052981) and the American Federation for Aging Research (AFAR) to D.M.H.; the Einstein Nathan Shock Center for Excellence in the Biology of Aging P30AG038072 and R37AG18381 to N.B.; P01AG031782 to A.M.C.; and R01GM108646 to D.S. D.E.L.P. received support from NIA grants R01AG049494 and R01AG013280. R.O.W. and T.T. are supported by a T32 Training Grant (T32AG23475) and A.D.H. is supported by T32GM007491. E.A. received support from the NIH/NIA P30AG038072 Pilot & Feasibility (P&F) Award and the NIH/National Institute of Diabetes and Digestive and Kidney Diseases (NIDDK) DK041296 P&F Award. This work was also supported by the Einstein-Sinai Diabetes Research Center (P30DK020541) and the National Cancer Institute (NCI)-supported Einstein Cancer Center (P30CA013330). The authors would like to acknowledge the Northwest Metabolomics Research Center and the valuable assistance of Lisa F. Bettcher, Dr. Robert Pepin, and Dr. Daniel Raftery in performing metabolomic data analysis. The authors would finally like to thank Dr. Pasha Apontes, Hongqian Liang, and Zunju Hu for technical assistance.

AUTHOR CONTRIBUTIONS

D.M.H. designed the study, analyzed the data, and wrote the manuscript. R.O.W. performed the experiments, analyzed the data, and wrote the manuscript. E.A., A.D., S.T., and A.M.C. performed the autophagy experiments, contributed to the experimental design, and wrote and edited the manuscript. K.M., D.W., A.D.H., F.G., T.T., and V.T. helped perform the experiments. L.F. provided human samples, contributed to the experimental design, and wrote and edited the manuscript. N.B. contributed to the experimental design and wrote and edited the manuscript. Y.Q., H.S., and I.J.K. contributed to the experimental design and performed the metabolomic experiments. D.E.L.P. and C.L.G. contributed to the experimental design, performed the metabolomic data analysis, and wrote the manuscript. D.S. and E.S.B. performed the experiments and wrote and edited the manuscript.

DECLARATION OF INTERESTS

The authors declare no competing interests.

Received: October 10, 2017
Revised: August 2, 2018
Accepted: September 19, 2018
Published: October 16, 2018

REFERENCES

Aida, K., Tawata, M., Negishi, M., and Onaya, T. (1997). Mouse glycine N-methyltransferase is sexually dimorphic and regulated by growth hormone. Horm. Metab. Res. *29*, 646–649.

Arias, E., Koga, H., Diaz, A., Mocholi, E., Patel, B., and Cuervo, A.M. (2015). Lysosomal mTORC2/PHLPP1/Akt Regulate Chaperone-Mediated Autophagy. Mol. Cell *59*, 270–284.

Barthel, F., Urban, A., Schlösser, L., Eulenburg, V., Werdehausen, R., Brandenburger, T., Aragon, C., Bauer, I., and Hermanns, H. (2014). Long-term application of glycine transporter inhibitors acts antineuropathic and modulates spinal N-methyl-D-aspartate receptor subunit NR-1 expression in rats. Anesthesiology *121*, 160–169.

Barzilai, N., Huffman, D.M., Muzumdar, R.H., and Bartke, A. (2012). The critical role of metabolic pathways in aging. Diabetes *61*, 1315–1322.

Benjamini, Y., Drai, D., Elmer, G., Kafkafi, N., and Golani, I. (2001). Controlling the false discovery rate in behavior genetics research. Behav. Brain Res. *125*, 279–284.

Bonhoure, N., Byrnes, A., Moir, R.D., Hodroj, W., Preitner, F., Praz, V., Marcelin, G., Chua, S.C., Jr., Martinez-Lopez, N., Singh, R., et al. (2015). Loss of the RNA polymerase III repressor MAF1 confers obesity resistance. Genes Dev. *29*, 934–947.

Brown-Borg, H.M., Rakoczy, S.G., and Uthus, E.O. (2005). Growth hormone alters methionine and glutathione metabolism in Ames dwarf mice. Mech. Ageing Dev. *126*, 389–398.

Brown-Borg, H.M., Rakoczy, S.G., Wonderlich, J.A., Rojanathammanee, L., Kopchick, J.J., Armstrong, V., and Raasakka, D. (2014). Growth hormone signaling is necessary for lifespan extension by dietary methionine. Aging Cell *13*, 1019–1027.

Burgos, E.S., Walters, R.O., Huffman, D.M., and Shechter, D. (2017). A simplified characterization of S-adenosyl-L-methionine-consuming enzymes with 1-Step EZ-MTase: a universal and straightforward coupled-assay for in vitro and in vivo setting. Chem. Sci. *8*, 6601–6612.

Cartier, A., Côté, M., Lemieux, I., Pérusse, L., Tremblay, A., Bouchard, C., and Després, J.P. (2009). Age-related differences in inflammatory markers in men: contribution of visceral adiposity. Metabolism *58*, 1452–1458.

Chen, K.T., Wu, C.H., Tsai, M.H., Wu, Y.C., Jou, M.J., Huang, C.C., and Wei, I.H. (2017). Antidepressant-like effects of long-term sarcosine treatment in rats with or without chronic unpredictable stress. Behav. Brain Res. *316*, 1–10.

Cheng, S., Larson, M.G., McCabe, E.L., Murabito, J.M., Rhee, E.P., Ho, J.E., Jacques, P.F., Ghorbani, A., Magnusson, M., Souza, A.L., et al. (2015). Distinct metabolomic signatures are associated with longevity in humans. Nat. Commun. *6*, 6791.

Cuervo, A.M., and Dice, J.F. (1996). A receptor for the selective uptake and degradation of proteins by lysosomes. Science *273*, 501–503.

De Guzman, J.M., Ku, G., Fahey, R., Youm, Y.H., Kass, I., Ingram, D.K., Dixit, V.D., and Kheterpal, I. (2013). Chronic caloric restriction partially protects against age-related alteration in serum metabolome. Age (Dordr.) *35*, 1091–1104.

de Vogel, S., Ulvik, A., Meyer, K., Ueland, P.M., Nygård, O., Vollset, S.E., Tell, G.S., Gregory, J.F., 3rd, Tretli, S., and Bjørge, T. (2014). Sarcosine and other metabolites along the choline oxidation pathway in relation to prostate cancer–a large nested case-control study within the JANUS cohort in Norway. Int. J. Cancer *134*, 197–206.

Felder, T.K., Ring-Dimitriou, S., Auer, S., Soyal, S.M., Kedenko, L., Rinnerthaler, M., Cadamuro, J., Haschke-Becher, E., Aigner, E., Paulweber, B., and Patsch, W. (2017). Specific circulating phospholipids, acylcarnitines, amino acids and biogenic amines are aerobic exercise markers. J. Sci. Med. Sport *20*, 700–705.

Fontana, L., Klein, S., and Holloszy, J.O. (2010a). Effects of long-term calorie restriction and endurance exercise on glucose tolerance, insulin action, and adipokine production. Age (Dordr.) *32*, 97–108.

Fontana, L., Partridge, L., and Longo, V.D. (2010b). Extending healthy life span–from yeast to humans. Science *328*, 321–326.

Gonzalez-Covarrubias, V., Beekman, M., Uh, H.W., Dane, A., Troost, J., Paliukhovich, I., van der Kloet, F.M., Houwing-Duistermaat, J., Vreeken, R.J., Hankemeier, T., and Slagboom, E.P. (2013). Lipidomics of familial longevity. Aging Cell *12*, 426–434.

Hasokawa, M., Shinohara, M., Tsugawa, H., Bamba, T., Fukusaki, E., Nishiumi, S., Nishimura, K., Yoshida, M., Ishida, T., and Hirata, K. (2012). Identification of biomarkers of stent restenosis with serum metabolomic profiling using gas chromatography/mass spectrometry. Circ. J. *76*, 1864–1873.

Hoffman, J.M., Soltow, Q.A., Li, S., Sidik, A., Jones, D.P., and Promislow, D.E. (2014). Effects of age, sex, and genotype on high-sensitivity metabolomic profiles in the fruit fly, Drosophila melanogaster. Aging Cell *13*, 596–604.

Hoffman, J.M., Tran, V., Wachtman, L.M., Green, C.L., Jones, D.P., and Promislow, D.E. (2016). A longitudinal analysis of the effects of age on the blood plasma metabolome in the common marmoset, Callithrix jacchus. Exp. Gerontol. *76*, 17–24.

Houtkooper, R.H., Argmann, C., Houten, S.M., Cantó, C., Jeninga, E.H., Andreux, P.A., Thomas, C., Doenlen, R., Schoonjans, K., and Auwerx, J. (2011). The metabolic footprint of aging in mice. Sci. Rep. *1*, 134.

Huffman, D.M., Johnson, M.S., Watts, A., Elgavish, A., Eltoum, I.A., and Nagy, T.R. (2007). Cancer progression in the transgenic adenocarcinoma of mouse prostate mouse is related to energy balance, body mass, and body composition, but not food intake. Cancer Res. *67*, 417–424.

Huffman, D.M., Farias Quipildor, G., Mao, K., Zhang, X., Wan, J., Apontes, P., Cohen, P., and Barzilai, N. (2016). Central insulin-like growth factor-1 (IGF-1) restores whole-body insulin action in a model of age-related insulin resistance and IGF-1 decline. Aging Cell *15*, 181–186.

Jentzmik, F., Stephan, C., Lein, M., Miller, K., Kamlage, B., Bethan, B., Kristiansen, G., and Jung, K. (2011). Sarcosine in prostate cancer tissue is not a differential metabolite for prostate cancer aggressiveness and biochemical progression. J. Urol. *185*, 706–711.

Johannsen, D.L., Conley, K.E., Bajpeyi, S., Punyanitya, M., Gallagher, D., Zhang, Z., Covington, J., Smith, S.R., and Ravussin, E. (2012). Ectopic lipid accumulation and reduced glucose tolerance in elderly adults are accompanied by altered skeletal muscle mitochondrial activity. J. Clin. Endocrinol. Metab. *97*, 242–250.

Jové, M., Naudí, A., Aledo, J.C., Cabré, R., Ayala, V., Portero-Otin, M., Barja, G., and Pamplona, R. (2013). Plasma long-chain free fatty acids predict mammalian longevity. Sci. Rep. *3*, 3346.

Jové, M., Maté, I., Naudí, A., Mota-Martorell, N., Portero-Otín, M., De la Fuente, M., and Pamplona, R. (2016). Human aging is a metabolome-related matter of gender. J. Gerontol. A Biol. Sci. Med. Sci. *71*, 578–585.

Karnovsky, A., Weymouth, T., Hull, T., Tarcea, V.G., Scardoni, G., Laudanna, C., Sartor, M.A., Stringer, K.A., Jagadish, H.V., Burant, C., et al. (2012). Metscape 2 bioinformatics tool for the analysis and visualization of metabolomics and gene expression data. Bioinformatics *28*, 373–380.

Kaushik, S., and Cuervo, A.M. (2009). Methods to monitor chaperone-mediated autophagy. Methods Enzymol. *452*, 297–324.

Kaushik, S., and Cuervo, A.M. (2015). Proteostasis and aging. Nat. Med. *21*, 1406–1415.

Kim, J., Kundu, M., Viollet, B., and Guan, K.-L. (2011). AMPK and mTOR regulate autophagy through direct phosphorylation of Ulk1. Nat. Cell Biol. *13*, 132–141.

Kim, S., Cheon, H.S., Song, J.C., Yun, S.M., Park, S.I., and Jeon, J.P. (2014). Aging-related changes in mouse serum glycerophospholipid profiles. Osong Public Health Res. Perspect. *5*, 345–350.

Kimura, S., Noda, T., and Yoshimori, T. (2007). Dissection of the autophagosome maturation process by a novel reporter protein, tandem fluorescent-tagged LC3. Autophagy *3*, 452–460.

Kind, T., Wohlgemuth, G., Lee, D.Y., Lu, Y., Palazoglu, M., Shahbaz, S., and Fiehn, O. (2009). FiehnLib: mass spectral and retention index libraries for metabolomics based on quadrupole and time-of-flight gas chromatography/mass spectrometry. Anal. Chem. *81*, 10038–10048.

Klionsky, D.J., Abdelmohsen, K., Abe, A., Abedin, M.J., Abeliovich, H., Acevedo Arozena, A., Adachi, H., Adams, C.M., Adams, P.D., Adeli, K., et al. (2016). Guidelines for the use and interpretation of assays for monitoring autophagy (3rd edition). Autophagy *12*, 1–222.

Koga, H., Martinez-Vicente, M., Arias, E., Kaushik, S., Sulzer, D., and Cuervo, A.M. (2011a). Constitutive upregulation of chaperone-mediated autophagy in Huntington's disease. J. Neurosci. *31*, 18492–18505.

Koga, H., Martinez-Vicente, M., Macian, F., Verkhusha, V.V., and Cuervo, A.M. (2011b). A photoconvertible fluorescent reporter to track chaperone-mediated autophagy. Nat. Commun. *2*, 386.

Koutros, S., Meyer, T.E., Fox, S.D., Issaq, H.J., Veenstra, T.D., Huang, W.Y., Yu, K., Albanes, D., Chu, L.W., Andriole, G., et al. (2013). Prospective evaluation of serum sarcosine and risk of prostate cancer in the Prostate, Lung, Colorectal and Ovarian Cancer Screening Trial. Carcinogenesis *34*, 2281–2285.

Kumar, V., Ahmad, M.A., Najmi, A.K., and Akhtar, M. (2016). Effect of sarcosine (a glycine transport 1 inhibitor) and risperidone (an atypical antipsychotic drug) on MK-801 induced learning and memory deficits in rats. Drug Res. (Stuttg.) *66*, 11–17.

Laye, M.J., Tran, V., Jones, D.P., Kapahi, P., and Promislow, D.E. (2015). The effects of age and dietary restriction on the tissue-specific metabolome of Drosophila. Aging Cell *14*, 797–808.

Lewis, K.N., Rubinstein, N.D., and Buffenstein, R. (2018). A window into extreme longevity; the circulating metabolomic signature of the naked mole-rat, a mammal that shows negligible senescence. Geroscience *40*, 105–121.

López-Ibáñez, J., Pazos, F., and Chagoyen, M. (2016). MBROLE 2.0-functional enrichment of chemical compounds. Nucleic Acids Res. *44*, W201–W204.

Luka, Z., Mudd, S.H., and Wagner, C. (2009). Glycine N-methyltransferase and regulation of S-adenosylmethionine levels. J. Biol. Chem. *284*, 22507–22511.

Ma, S., Yim, S.H., Lee, S.G., Kim, E.B., Lee, S.R., Chang, K.T., Buffenstein, R., Lewis, K.N., Park, T.J., Miller, R.A., et al. (2015). Organization of the mammalian metabolome according to organ function, lineage specialization, and longevity. Cell Metab. *22*, 332–343.

Madeo, F., Zimmermann, A., Maiuri, M.C., and Kroemer, G. (2015). Essential role for autophagy in life span extension. J. Clin. Invest. *125*, 85–93.

Mao, K., Quipildor, G.F., Tabrizian, T., Novaj, A., Guan, F., Walters, R.O., Delahaye, F., Hubbard, G.B., Ikeno, Y., Ejima, K., et al. (2018). Late-life targeting of the IGF-1 receptor improves healthspan and lifespan in female mice. Nat. Commun. *9*, 2394.

Meyer, T.E., Kovács, S.J., Ehsani, A.A., Klein, S., Holloszy, J.O., and Fontana, L. (2006). Long-term caloric restriction ameliorates the decline in diastolic function in humans. J. Am. Coll. Cardiol. *47*, 398–402.

Mitchell, T.W., Buffenstein, R., and Hulbert, A.J. (2007). Membrane phospholipid composition may contribute to exceptional longevity of the naked mole-rat (Heterocephalus glaber): a comparative study using shotgun lipidomics. Exp. Gerontol. *42*, 1053–1062.

Obata, F., and Miura, M. (2015). Enhancing S-adenosyl-methionine catabolism extends Drosophila lifespan. Nat. Commun. *6*, 8332.

Orentreich, N., Matias, J.R., DeFelice, A., and Zimmerman, J.A. (1993). Low methionine ingestion by rats extends life span. J. Nutr. *123*, 269–274.

Pinto, M.C., Simão, F., da Costa, F.L., Rosa, D.V., de Paiva, M.J., Resende, R.R., Romano-Silva, M.A., Gomez, M.V., and Gomez, R.S. (2014). Sarcosine preconditioning induces ischemic tolerance against global cerebral ischemia. Neuroscience *271*, 160–169.

Pontoizeau, C., Mouchiroud, L., Molin, L., Mergoud-Dit-Lamarche, A., Dallière, N., Toulhoat, P., Elena-Herrmann, B., and Solari, F. (2014). Metabolomics analysis uncovers that dietary restriction buffers metabolic changes associated with aging in Caenorhabditis elegans. J. Proteome Res. *13*, 2910–2919.

Richie, J.P., Jr., Leutzinger, Y., Parthasarathy, S., Malloy, V., Orentreich, N., and Zimmerman, J.A. (1994). Methionine restriction increases blood glutathione and longevity in F344 rats. FASEB J. *8*, 1302–1307.

Ruckenstuhl, C., Netzberger, C., Entfellner, I., Carmona-Gutierrez, D., Kickenweiz, T., Stekovic, S., Gleixner, C., Schmid, C., Klug, L., Sorgo, A.G., et al. (2014). Lifespan extension by methionine restriction requires autophagy-dependent vacuolar acidification. PLoS Genet. *10*, e1004347.

Schneider, J.L., Villarroya, J., Diaz-Carretero, A., Patel, B., Urbanska, A.M., Thi, M.M., Villarroya, F., Santambrogio, L., and Cuervo, A.M. (2015). Loss of hepatic chaperone-mediated autophagy accelerates proteostasis failure in aging. Aging Cell *14*, 249–264.

Soare, A., Cangemi, R., Omodei, D., Holloszy, J.O., and Fontana, L. (2011). Long-term calorie restriction, but not endurance exercise, lowers core body temperature in humans. Aging (Albany N.Y.) *3*, 374–379.

Socała, K., Nieoczym, D., Rundfeldt, C., and Wlaź, P. (2010). Effects of sarcosine, a glycine transporter type 1 inhibitor, in two mouse seizure models. Pharmacol. Rep. *62*, 392–397.

Sreekumar, A., Poisson, L.M., Rajendiran, T.M., Khan, A.P., Cao, Q., Yu, J., Laxman, B., Mehra, R., Lonigro, R.J., Li, Y., et al. (2009). Metabolomic profiles delineate potential role for sarcosine in prostate cancer progression. Nature *457*, 910–914.

Stein, P.K., Soare, A., Meyer, T.E., Cangemi, R., Holloszy, J.O., and Fontana, L. (2012). Caloric restriction may reverse age-related autonomic decline in humans. Aging Cell *11*, 644–650.

Strzelecki, D., Podgórski, M., Kałużyńska, O., Stefańczyk, L., Kotlicka-Antczak, M., Gmitrowicz, A., and Grzelak, P. (2015). Adding sarcosine to antipsychotic treatment in patients with stable schizophrenia changes the concentrations of neuronal and glial metabolites in the left dorsolateral prefrontal cortex. Int. J. Mol. Sci. *16*, 24475–24489.

Sutter, B.M., Wu, X., Laxman, S., and Tu, B.P. (2013). Methionine inhibits autophagy and promotes growth by inducing the SAM-responsive methylation of PP2A. Cell *154*, 403–415.

Svingen, G.F., Schartum-Hansen, H., Pedersen, E.R., Ueland, P.M., Tell, G.S., Mellgren, G., Njølstad, P.R., Seifert, R., Strand, E., Karlsson, T., and Nygård, O. (2016). Prospective associations of systemic and urinary choline metabolites with incident type 2 diabetes. Clin. Chem. *62*, 755–765.

Trayssac, M., Hannun, Y.A., and Obeid, L.M. (2018). Role of sphingolipids in senescence: implication in aging and age-related diseases. J. Clin. Invest. *128*, 2702–2712.

Tsai, G., Lane, H.Y., Yang, P., Chong, M.Y., and Lange, N. (2004). Glycine transporter I inhibitor, N-methylglycine (sarcosine), added to antipsychotics for the treatment of schizophrenia. Biol. Psychiatry *55*, 452–456.

Tsai, C.H., Huang, H.C., Liu, B.L., Li, C.I., Lu, M.K., Chen, X., Tsai, M.C., Yang, Y.W., and Lane, H.Y. (2014). Activation of N-methyl-D-aspartate receptor glycine site temporally ameliorates neuropsychiatric symptoms of Parkinson's disease with dementia. Psychiatry Clin. Neurosci. *68*, 692–700.

Uthus, E.O., and Brown-Borg, H.M. (2003). Altered methionine metabolism in long living Ames dwarf mice. Exp. Gerontol. *38*, 491–498.

Wagner, J., Claverie, N., and Danzin, C. (1984). A rapid high-performance liquid chromatographic procedure for the simultaneous determination of methionine, ethionine, S-adenosylmethionine, S-adenosylethionine, and the natural polyamines in rat tissues. Anal. Biochem. *140*, 108–116.

Wennberg, A.M.V., Schafer, M.J., LeBrasseur, N.K., Savica, R., Bui, H.H., Hagen, C.E., Hollman, J.H., Petersen, R.C., and Mielke, M.M. (2018). Plasma sphingolipids are associated with gait parameters in the Mayo Clinic Study of Aging. J. Gerontol. A Biol. Sci. Med. Sci. *73*, 960–965.

Xia, J., and Wishart, D.S. (2010). MSEA: a web-based tool to identify biologically meaningful patterns in quantitative metabolomic data. Nucleic Acids Res. *38*, W71–W77.

Zubiete-Franco, I., García-Rodríguez, J.L., Martínez-Uña, M., Martínez-Lopez, N., Woodhoo, A., Juan, V.G., Beraza, N., Lage-Medina, S., Andrade, F., Fernandez, M.L., et al. (2016). Methionine and S-adenosylmethionine levels are critical regulators of PP2A activity modulating lipophagy during steatosis. J. Hepatol. *64*, 409–418.

STAR★METHODS

KEY RESOURCES TABLE

REAGENT or RESOURCE	SOURCE	IDENTIFIER
Antibodies		
Mouse anti-Acetylated Tubulin	Sigma-Aldrich	Cat# T7451; RRID: AB_609894
Mouse anti-Actin	Sigma-Aldrich	Cat# A2172; RRID: AB_2211260
Rabbit anti-p62	Enzo Life Sciences	Cat# BML-PW9860; RRID: AB_2196009
Rabbit anti-LC3B	Cell Signaling Technology	Cat# 2775S; RRID:AB_915950
Mouse anti-S6	N/A	Cat# 2217S; RRID: AB_331355
Rabbit anti-pS6	N/A	Cat# 5364S; RRID: AB_10694233
Rabbit anti-Akt	N/A	Cat# 4691L; RRID: AB_915783
Rabbit anti-pAkt	N/A	Cat# 9271S; RRID: AB_329825
Rabbit anti-Ulk	N/A	Cat# 8054; RRID: AB_11178668
Rabbit anti-pUlk	N/A	Cat# 5869; RRID: AB_10707365
Rabbit anti-pmTOR	N/A	Cat# 5536S; RRID: AB_10691552
Rabbit anti-mTOR	N/A	Cat# 2983S; RRID: AB_2105622
Rabbit anti-pAMPK	N/A	Cat# 2532; RRID: AB_330331
Rabbit anti-AMPK	N/A	Cat# 2535; RRID: AB_331250
Rat anti-LAMP1	Developmental Hybridoma Bank	Cat# 1D4B; RRID: AB_2134500
Rat anti-LAMP2A	Cuervo and Dice (1996)	N/A
Rabbit-anti-GNMT	AbCam	Cat# ab203396
Mouse anti-GAPDH	AbCam	Cat# ab8245; RRID: AB_2107448
Anti-Rabbit HRP Conjugate	Seracare (KPL)	Cat# 074-15-061
Anti-Mouse HRP Conjugate	Seracare (KPL)	Cat# 074-18-061
Bacterial and Virus Strains		
E. coli DH5α	ATCC	N/A
Chemicals, Peptides, and Recombinant Proteins		
Ammonium chloride	Sigma-Aldrich	Cat# A9434
Leupeptin	Fisher BioReagents	Cat# BP26625
cOmplete, EDTA-free Protease Inhibitor Cocktail	Sigma-Aldrich (Merck)	Cat# 0000000050564 89001
PhosSTOP	Sigma-Aldrich (Merck)	Cat# 0000000049068 45001
Sarcosine	Sigma Aldrich	Cat# 84532
BioRad Criterion TGX 4-20% Stain Free Gels	BioRad	Cat# 5678095
Pierce ECL Western Blotting Substrate	Thermo Fisher Scientific	Cat# 32106
Fluoromount-G, with DAPI	Invitrogen (Thermo Fisher Scientific)	Cat# 00-4959-52
Fluoromount-G	Invitrogen (Thermo Fisher Scientific)	Cat#00-4958-02
Formaldehyde solution, 37wt	Sigma-Aldrich (Merck)	Cat# 252549
Methanol	Sigma-Aldrich (Merck)	Cat# 322415
Critical Commercial Assays		
Biocrates AbsoluteIDQ p180 kit	BIOCRATES Life Sciences	N/A
Sarcosine Fluorescence Assay	Cell Technology	SARC100
Experimental Models: Cell Lines	N/A	N/A
Human: NIH 3T3 mouse fibroblasts	Coriell Institute	N/A
Recombinant DNA		
pDEST-mCherry-EGFP-LC3B	Dr. Terje Johansen (University of Trømso, Trømso, Norway)	N/A
KFERQ-Dendra	Cuervo lab	N/A

(*Continued on next page*)

Continued

REAGENT or RESOURCE	SOURCE	IDENTIFIER
Software and Algorithms		
Fiji	NIH	http://fiji.sc/; RRID: SCR_002285
AxioVision Rel. 4.8	Carl Zeiss	https://www.zeiss.com; RRID: SCR_002677
LAS AF Lite	Leica	https://www.leica-microsystems.com; RRID: SCR_013673
Adobe Photoshop 6.0	Adobe Systems	https://www.adobe.com; RRID: SCR_014199
Green and Red Puncta Colocalization Macro	D. J. Swiwarski modified by R.K. Dagda	http://imagejdocu.tudor.lu/doku.php?id=plugin:analysis:colocalization_analysis_macro_for_red_and_green_puncta:start
GraphPad Prism 6.0	GraphPad Software	https://www.graphpad.com/scientific-software/prism/; RRID: SCR_002798
Primer Express v.2.0	Applied Biosystems (Thermo Fisher Scientific)	https://www.thermofisher.com/us/en/home/brands/applied-biosystems.html; RRID: SCR_014326
Image Lab v6	Biorad	N/A
R Statistical Package	N/A	https://www.r-project.org/
SPSS v16	SPSS	N/A
SigmaPlot v10	Systat Software	N/A
Other		
Fujifilm LAS-3000 Imager	Fujifilm, Albert Einstein College of Medicine	http://www.fujifilm.com/products/medical/
Axiovert 200 with ApoTome 0.2 system fluorescence microscope	Carl Zeiss, Albert Einstein College of Medicine	https://www.zeiss.com
SP5-MP-FLIM confocal microscope	Leica, Bordeaux Imaging Centre	https://www.leica-microsystems.com
JEOL 1200EX transmission electron microscope	JEOL USA	N/A
BioRad Chemidoc MP	BioRad	N/A

CONTACT FOR REAGENT AND RESOURCE SHARING

Further information and requests for resources and reagents should be directed to and will be fulfilled by the Lead Contact, Derek M. Huffman, PhD (derek.huffman@einstein.yu.edu).

EXPERIMENTAL MODEL AND SUBJECT DETAILS

Fischer 344 x Brown Norway (FBN) F1 hybrid male rats were obtained from the NIA aging rodent colony and housed under standard temperature and photoperiod conditions. For DR studies, young FBN rats were obtained at 3 months of age and assigned to AL feeding (YAL n = 8) or 40% DR (YDR n = 8), which was gradually imposed over a 3 week period and maintained until 6-7 months of age. Aged AL and DR FBN rats were obtained at 19 months of age from NIA and were maintained on these regimens until 22-23 months of age. All animals were individually housed and provided a weighed amount of rodent chow (Purina 5001). AL intake was monitored on a weekly basis by measuring the disappearance of food, while DR animals were provided a weighed amount of pellets (12 g) each afternoon. Serum from 4 mo and 24 mo old female control and Ames dwarf mice (n = 8 group) were obtained from the NIA Rodent Tissue Bank. In brief, Ames dwarf mouse serum was separated from whole blood samples collected via cardiac puncture under anesthesia by CO_2 inhalation and stored in 200uL aliquots at −80°C. For characterizing age-related changes in sarcosine and sarcosine feeding studies, male FBN rats were obtained at 4, 12 and 24 mo of age, respectively.

In humans, the metabolome was determined for shared metabolomic changes in a similarly designed set of serum samples obtained following an overnight fast from a well-characterized cohort of relatively younger and older subjects consuming a Western Diet (WD) or a self-imposed DR diet, whereby individual Kcal intake was approximately 30% less than that reported in the WD group for an average of 7-15 years (Fontana et al., 2010a; Soare et al., 2011; Stein et al., 2012). The group characteristics were as follows: 1) younger WD: n = 6 (5M, 1F), age = 38.0 ± 2.8yrs; 2) younger DR: n = 6 (6M), age = 37.8 ± 2.6yrs; 3) older

WD: n = 7 (6M, 1F), age = 64.6 ± 1.6yrs; 4) older DR: n = 7 (5M, 2F) age = 65.0 ± 1.4yrs. All animal experiments were approved by the Institutional Animal Care and Use Committee at the Albert Einstein College of Medicine. All human studies were approved by the Institutional Review Board at Washington University in St. Louis.

METHOD DETAILS

Basic physiology characteristics

Beginning at 3 months and 19 months of age, respectively, body weight and food intake were monitored on a weekly basis. Prior to sacrifice, body composition was determined by quantitative magnetic resonance (qMR; Echo Medical Systems, Houston, TX). At study completion, animals were fasted at approximately 0800hr for 4-6 hr prior to being anesthetized under isoflurane and sacrificed. Trunk blood was collected and tissues were rapidly freeze clamped and flash frozen in liquid nitrogen for downstream applications. Whole blood was collected into K^+ EDTA collection tubes and plasma was separated by centrifugation at 1,500 x g at 4°C for 15 min and stored at −80°C. Rat plasma insulin was measured by a rat/mouse ELISA (EMD Millipore, Inc) with rat insulin standards. FFA (Wako, Diagnostics, Richmond, VA), TG, and free glycerol (Sigma, St. Louis, MO) were analyzed in technical triplicates using standard calorimetric assays.

Indirect calorimetry

Energy expenditure, substrate utilization and spontaneous activity were determined by indirect calorimetry as described (Huffman et al., 2016; Huffman et al., 2007), based upon O_2 consumption and CO_2 production, using a Rat Oxymax System (Columbus Instruments, Columbus, OH). In brief, YAL and OAL and DR animals (n = 8 per group) were placed into individual cages and allowed to acclimate for at least 72 hr prior to the experiment. DR animals were provided 12 g of food pellets at 1200h while AL animals were provided unlimited access to feed. Beginning at 1700h, data were collected over 24 hr, and at 1700h the next day, animals were fasted overnight to evaluate metabolic fuel switching during energy deprivation.

Sarcosine feeding studies

Sarcosine (N-methyl glycine) was purchased from Sigma (cat#84532) and incorporated into Purina chow 5001 at a concentration of 1250 mg/kg (Research Diets, Inc). Control and sarcosine-supplemented diets, respectively, were subsequently provided AL to 24 mo old male FBN rats for either 10 days (short-term experiments) as well as 4 wk and 8 wk chronic studies. Body weight and food intake were monitored throughout and body composition was assessed prior to sacrifice by qMR in the 8 wk cohort. For some animals in the 10-day feeding cohort, jugular catheters were inserted prior to initiating sarcosine feeding (n = 3) to allow for serial blood collection at 0900h, 1200h, 1500h and 1800h, respectively, in serum collection tubes (Sarstedt Inc; Numbecht, Germany) for later *in vitro* autophagy studies. At study completion, animals were sacrificed in a similar manner as described for the aging and diet cohort study. Food was removed at 0800hr for 4-6 hr prior to being anesthetized under isoflurane, and animals were sacrificed for collection of trunk blood and tissues for analyses. Whole blood was collected into K^+ EDTA collection tubes and plasma was separated by centrifugation at 1,500 x g for 15 min at 4°C and stored at −80°C.

In vivo sarcosine regulation studies

In order to more carefully characterize to what extent sarcosine levels may be regulated *in vivo*, we assessed plasma levels across several ages from trunk blood obtained following a 4 hr fast using a fluorescent-based sarcosine assay (described below) in Young (4 mo; n = 8), Middle Aged (12 mo; n = 8) and Old (25-26 mo; n = 10) male FBN rats. In addition, plasma sarcosine levels were evaluated in venous blood collected from an indwelling catheter at several time points to characterize levels throughout the day, as well as under fed and fasted conditions, in 4-5 mo old FBN male rats. Specifically, animals were sedated with 2% isoflurane for surgical placement of an indwelling catheter into the right internal jugular vein, similar as described (Huffman et al., 2016). Rats were then singly housed and treated with analgesic as needed and monitored until body weight returned to within 3% of preoperative levels (~7 days). For time course studies, catheterized animals (n = 8) remained in their home cage and had continuous access to food and water throughout the day. Venous blood (~500uL) was then collected from awake, unstressed rats at 0700, 1100, 1500 and 1900hr, respectively, and plasma was rapidly separated and stored at −80°C. For the fasting/re-feeding study, animals were assigned to either Control (n = 7) or overnight Fasting (n = 7) conditions. Rats were then moved to a clean home cage 1 hr prior to beginning the study, and a baseline venous blood sample was collected at 1700hr. Control animals were then allowed continuous, AL access to food and water overnight, while rats assigned to the Fasting group were subjected to an overnight food only deprivation beginning at 1700h with access to water. At 0900hr, a second venous blood sample was collected, and food was then returned to the home cage of fasted animals for 3 hr, and a third venous sample was collected at 1200hr after 3hrs refeeding, and plasma was rapidly separated and stored at −80°C for analysis.

Quantitation of SAM and SAH levels in plasma and liver

The SAM methyl cofactor and its SAH methyltransferase product were analyzed in plasma by Creative Proteomics Inc. (Shirley, NY). In brief, plasma samples were spiked with internal standard solution in 0.1% formic acid and then treated with 70% perchloric acid. Following acid extraction, supernatants were analyzed by HPLC-tMS in the multiple reaction monitoring (MRM) setting. For liver SAM

and SAH, analysis was performed by HPLC from acid extracted rat liver samples according to previous described methods (Wagner et al., 1984), with slight modifications. In brief, frozen livers (250 mg) were pulverized and extracted with 1mL 0.2M perchloric acid. Samples were then centrifuged and supernatants were diluted 5x with HPLC Buffer A prior to injection (50 μL). Metabolites were resolved at 40°C onto a reverse phase column (Luna $C18^2$-HTS, 2.5 μm, 100 Å, 100 × 2 mm; # 00D-4446-B0, Phenomenex) using a phosphate/octanesulfonate buffer gradient (Flow 0.30 mL min^{-1}; Time, Buffer A/B percentage: 0–2 min 85/15, 2–14 min 0/100, 14–21 min 0/100, 21–21.5 min 85/15, 21.5–30 min 85/15). Both SAH and SAM were characterized by a maximum absorption at 256 nm and eluted at 11.39 and 12.76 min, respectively; such detection was linear across a 5–140 pmol range.

Protein isolation and western blotting

Total protein was mechanically homogenized and extracted with denaturing lysis buffer (150mM NaCl, 50mM Tris-HCl (pH 7.4), 0.25% DOC, 5mM EDTA, 1% Triton X-100, 1mM orthovanadate, 100mM NaF, 5mM Na Pyrophosphate, 1x PIC, and 100uM PMSF) and protein content was determined using the BCA protein assay (Sigma, St. Louis, MO) with BSA as a standard, as described (Mao et al., 2018). Proteins were separated by SDS-PAGE using Bis-Tris stain-free gels (BioRad, Hercules, CA), and total protein was imaged and quantified to confirm equal loading. Gels were then wet-transferred onto PVDF membranes at 100V constant for 1hr, blocked with 5% milk or BSA, and incubated with an appropriate primary antibody against GNMT (Abcam #ab203396), mTOR (Cell Signaling #2983S), p-mTOR (Cell Signaling #5536S), Akt (Cell Signaling #4691L), pAktSer473 (Cell Signaling #9271S), S6 (Cell Signaling #2217S), pS6 (Cell Signaling #5364S), AMPK (Cell Signaling #2532), pAMPK (Cell Signaling #2535), Ulk1 (Cell Signaling #8054), pUlk (Cell Signaling #5869), LAMP1 (Developmental Studies Hybridoma Bank; 1D4B), or LAMP-2A (Cuervo and Dice, 1996) overnight at 4°C. Following a 1hr incubation with secondary antibody, bands were visualized by chemiluminescence using either an LAS-3000 Imaging System (Fijufim) for experiments in cells or a BioRad Chemidoc Bioimager for *in vivo* experiments to first pixel saturation and densitometry performed using software provided by the manufacturer.

EZ-MTase coupled assay for liver GMNT activity

Liver lysate was mechanically extracted with non-denaturing lysis buffer (150mM NaCl, 20mM Tris-HCl (pH 7.4), 1% Triton X-100, 1mM Orthovanadate, 10mM NaF, 1x PIC, 1mM PMSF) and protein content was determined using the BCA protein assay (Sigma, St. Louis, MO) with BSA as a standard. GNMT activity within rat liver extracts was quantified using the 1-Step EZ-MTase coupled assay through its UV-mode of detection (Burgos et al., 2017). The methyltransfer from SAM onto the glycine substrate generates sarcosine and SAH. The SAH product is further catabolized into *S*-inosyl-L-homocysteine (SIH) by the deaminase TM0936 and the decrease of absorbance at 263 nm is reporting on the methyltransfer reaction. Reactions were performed in 96-well plates (Greiner Bio-One, UV-Star® Microplate #655801) and absorbance was recorded onto a SpectraMax M5 (Molecular Devices). A master mix was combined with increasing volumes of liver extract, and blinded measurements were performed in duplicate. Methyltransfer reactions started upon addition of SAM (1.76 mM). Initial rates were plotted against liver extract volumes to yield a linear activity curve; the slope of this representation ($\mu M\ h^{-1}\ \mu L^{-1}$) was converted into GNMT activity and normalized to the amount of total protein originally present within liver extract (GNMT activity expressed in picomoles of sarcosine synthesized per minute and per milligram of total protein: pmol min^{-1} mg^{-1}) with a Z'-factor of 0.75 (Burgos et al., 2017).

Cells

Mouse fibroblasts (NIH 3T3) were obtained from the American Type Culture Collection (ATCC). Cells were maintained in Dulbecco's modified Eagle's medium (Sigma, St. Louis MO) in the presence of 10% newborn calf serum, 50 μg/ml penicillin and 50 μg/ml streptomycin at 37°C with 5% CO_2.

Autophagy analysis

Autophagy reporters were generated by transducing intact cells with lentivirus carrying the mCherry-GFP-LC3 tandem construct to measure macroautophagy activity *in vitro* (Kimura et al., 2007). Cells were plated on coverslips or glass-bottom 96-well plates and fluorescence recorded from both channels. Puncta positive for both fluorophores correspond to autophagosomes whereas those only positive for the red fluorophore correspond to autolysosomes. Autophagic flux was determined as the conversion of autophagosomes (yellow) to autolysosomes (red puncta). To measure CMA activity in intact cells, the photoactivatable KFERQ-PSDendra2 reporter was transduced into cells using lentiviral delivery (Koga et al., 2011a). Cells were photoactivated with a 405nm light emitting diode (Norlux) for 4min with the intensity of 3.5mA (constant current).

CMA activity was quantified as number of puncta per cell. Autophagy reporters were analyzed using high-content microscopy. Cells plated in glass-bottom 96-well plates were treated for the indicated times and following fixation, images were acquired using a high-content microscope (Operetta, Perkin Elmer). Images of 9 different fields per well were captured resulting in an average of 2,500-3,000 cells. Nuclei and puncta were identified using the manufacturer's software. The number of particles/puncta per cell was quantified using the "particle identifier" function in the cytosolic region after thresholding in non-saturated images (Kaushik & Cuervo, 2009; Arias et al., 2015). In all cases, focal plane thickness was set at 0.17 μm and sections with maximal nuclear diameter were selected for quantification. Values are presented as number of puncta per cell section which, in our acquisition conditions, represented 10%–20% of the total puncta per cell.

As an alternative method, macroautophagy flux was also measured as the amount of p62 degraded in lysosomes. Specifically, cells were treated with 20mM NH_4Cl and 100 μM leupeptin for 4 hours and then subjected to SDS-PAGE and immunoblotting for p62. Where indicated, autophagic flux in rat liver was measured *ex vivo* as previously described (Schneider et al., 2015). Briefly, freshly isolated livers were minced in $1mm^3$ cubes and incubated in DMEM either supplemented with or without 20mM NH_4Cl and 100 μM leupeptin for 2h at 37°C. Samples were then subjected to SDS-PAGE and immunoblot for p62 and LC3-II.

Transmission electron microscopy

Electron microscopy for liver was done after fixation of liver blocks (1 mm^3 in size) with 2% paraformaldehyde and 2% gluteraldehyde in 0.1M sodium cacodylate buffer followed by postfixation staining with 1% osmium tetroxide and 1% uranyl acetate. After dehydration, resin embedding and ultrathin sectioning, samples were viewed on a JEOL 1200EX transmission electron microscope at 80 kV (JEOL USA, Inc). Morphometric classification of autophagic vacuoles was done following standard criteria(Klionsky et al., 2016). Autophagosomes were distinguished as double membrane vesicles with content of similar density as the surrounding cytosol and comprised often of recognizable cellular structures. Autophagolysosomes were identified as single or partially double membrane vesicles of content of lower density than the surrounding cytosol and comprised of amorphous content or partially degraded cellular structures. In both cases, the limiting membrane had to be denuded of ribosomal particles. Morphometric analysis of autophagic compartments was done by double-blinded independent observers using a single-category allocation or each vesicle in at least 20 different micrographs per condition.

Metabolite profiling and quantification

For initial metabolomic studies, tissue samples were homogenized with 6 fold of 5mM ammonium acetate (liver) or 2.5mM ammonium acetate (brown fat and gastrocnemius). After two freeze-thaw cycles, 10uL (plasma, serum, and liver) or 20uL (brown fat and gastrocnemius) of extract was used for the Biocrates AbsoluteIDQ p180 kit as described (Bonhoure et al., 2015). The samples were analyzed with UPLC-MS/MS (Xevo TQ, Waters, Pittsburgh, PA, USA) in the Einstein Stable Isotope and Metabolomics Core according to the manufacturer's instructions (BIOCRATES Life Sciences AG, Innsbruck, Austria). In addition, an untargeted small metabolite screen was performed in human serum and rat plasma by GC/MS using an Agilent 7890a GC with a Gerstel automatic liner exchange cooled injection system CIS 4 PTV injector. Both split and large volume injections (LVI) of the sample were made. GC/MS conditions were set based on the Feihn protocol (Kind et al., 2009). Briefly, a 30 m DB-5MS column was used for metabolite separation. The oven program was started at 600°C, kept for 1min, and raise to 3200°C at the rate of 100°C/min and kept for 5min. Metabolite identification was done as described using NIST 11 and Fiehn mass spectral libraries. Pooled QC samples were used to evaluate the analytical variations based on the coefficient of variation (CV) from typically 6 or more injections.

Metabolites specifically related to folate, Met, glycine, and sarcosine pathways were evaluated in plasma from Old Control (n = 10) and Old Sarcosine (n = 10) animals following 4wks on diet at the Northwest Metabolomics Research Center. Specifically, samples were subjected to targeted LC-MS/MS analysis on a system consisting of Shimadzu Nexera XR LC-20AD pumps coupled to a Sciex 6500+ triple quadrupole mass spectrometer. The samples were separated on a Waters XBridge BEH column operated in a HILIC mode. The MS was operated in a scheduled MRM mode through Analyst v1.6.3. Metabolite concentrations were quanitified using the Multiquant 3.0 software.

Fluorescent detection of plasma sarcosine

Sarcosine from plasma samples was measured in a single-detection format by fluorescence with a coupled assay (Cell Technology, Freemont, CA; #SARC100). Briefly, in a 96-well plate (Corning, #3991), the enzyme reaction mixture (sarcosine oxidase and chemical probe, 50 μL) was added to both sarcosine standards (50 μL; 0-20 μM) and diluted samples (1:5, 50 μL; previously incubated at 60°C for 30 min). After centrifugation (1500 rpm, 2 min), fluorescent signal (545 nm excitation and 585 nm emission) was monitored onto a SpectraMax M5 plate reader (Molecular Devices).

QUANTIFICATION AND STATISTICAL ANALYSIS

All non-metabolomic, parametric data were analyzed either by independent samples t test, one-way ANOVA or two-way ANOVA (Age x Diet). When a significant main effect or interaction term, respectively, was observed, planned contrasts were performed with Tukey Honest Significant Difference [HSD] method. Longitudinal measures were assessed by two-way repeated-measures ANOVA (Group x Time) or three-way repeated-measures ANOVA (Age x Diet x Time), respectively, with repeated-measures on time, and within-subject effects were determined with Greenhous-Geisser adjustment. When a significant interaction term was observed, post hoc comparisons were performed on the mean difference with Tukey HSD adjustment. All data were analyzed using SPSS (SPSS Inc, Chicago, IL). Data were log transformed when necessary to ensure normality of distribution. A $p \leq 0.05$ was considered statistically significant for all analyses.

Metabolomic data analysis

For both human and rat populations, age and diet were categorized as dichotomous variables. Data were assigned by diet as either AL or diet restriction (DR), and by age in humans as younger (range = 27-46yrs) and older (range 58-71yrs), while rats were

categorized as young (~6mo) or old (22-23mo). Analyses were carried out separately for each sample type (human serum, rat plasma, rat liver, rat BAT, and rat SkM). Across the entire metabolome, data are log-normally distributed. Accordingly, prior to analysis, all data were log-transformed. Metabolites with more than two missing values were removed from the dataset. For univariate analysis, all samples were then centered such that the mean of all metabolites within a sample was equal to zero. For each metabolite, we then used a simple linear model,

$$\widehat{y_i} = \alpha + \beta_1 age + \beta_2 diet + \varepsilon$$

to test for significant effects of age and diet on each metabolite, where $\widehat{y_i}$ is the predicted value of the i^{th} metabolite as a function of diet and age. The sign and magnitude of the effect of age and DR on metabolite level is given by β_1 and β_2, respectively. To determine whether DR reverses the effect of age on metabolite levels, we compare β_1 and β_2 values for all metabolites within a particular sample.

Multivariate analysis was carried out in three stages. First, results from the univariate model were used to construct heatmaps. Each row represented a sample (clustered by age and diet), and each column represented a metabolite (clustered by statistical significance). We then carried out metabolite-set enrichment analysis (MSEA, (Xia and Wishart, 2010)) using the Enrichment Analysis package in MBROLE 2.0 (López-Ibáñez et al., 2016), comparing Human Metabolite Data Base (HMDB) lists for significant age or diet effects using the Benjamini-Hochberg method (Benjamini et al., 2001). Unless otherwise stated, significance for individual metabolites with p values $\leq$ 0.05 was determined with an FDR α = 0.1. Where significance depends on a higher FDR, this has been stated. We also used results from the univariate model described above to construct metabolite networks in Metscape (Karnovsky et al., 2012).

In a final step for multivariate analysis, we carried out principle component analysis (PCA) using the ord function from the made4 library in R. In this case, we removed any features with more than three missing values. Data were centered and scaled first by sample, and then by feature. We then imputed missing values using the impute.knn function in the impute library in R. We then used the topgenes function to identify metabolites with high loadings on significant principle components.

Creation of metabolic networks

To visualize metabolic pathways for both rat and human networks for changes with both age and diet, we used the MetScape 3 app for Cytoscape (version 3.4.0). Kyoto Encyclopedia of Genes and Genomes (KEGG) IDs, in addition to corresponding p values and fold changes were uploaded to Cytoscape. MetScape used inputted IDs to create networks where nodes are metabolites and direct edges indicate reactions converting them. Metabolites that increased were colored red, while decreased metabolites were colored blue, and significant metabolites were outlined in orange.

DATA AND SOFTWARE AVAILABILITY

All metabolomic data are freely available in Supplemental Files, and all other raw data as well as the R code files used for data analysis are available upon request.

Cell Reports, Volume *25*

Supplemental Information

Sarcosine Is Uniquely Modulated by Aging and Dietary Restriction in Rodents and Humans

Ryan O. Walters, Esperanza Arias, Antonio Diaz, Emmanuel S. Burgos, Fangxia Guan, Simoni Tiano, Kai Mao, Cara L. Green, Yungping Qiu, Hardik Shah, Donghai Wang, Adam D. Hudgins, Tahmineh Tabrizian, Valeria Tosti, David Shechter, Luigi Fontana, Irwin J. Kurland, Nir Barzilai, Ana Maria Cuervo, Daniel E.L. Promislow, and Derek M. Huffman

SUPPLEMENTARY MATERIALS

Figure S1 (Related to Figure 2). Human serum significant interactions with age and diet.

A

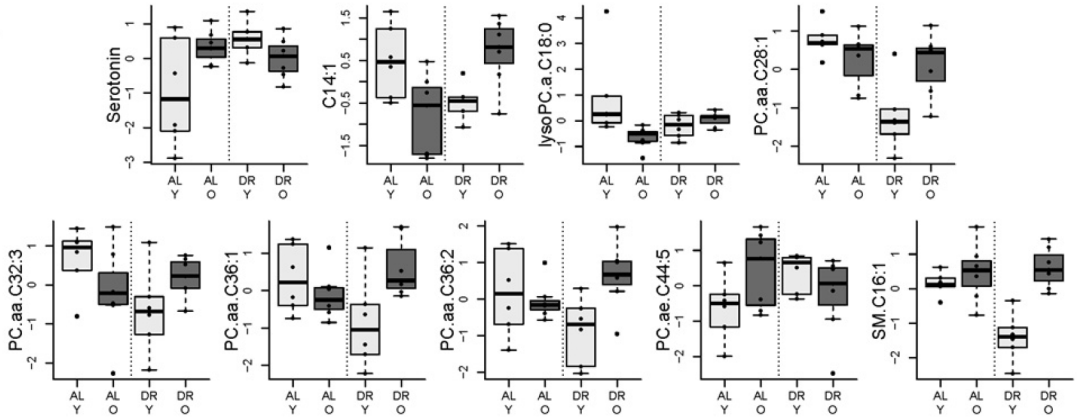

B

mz.id	beta.age	pval.age	beta.diet	pval.diet	beta.int	pval.int
C14:1	1.2866	0.00885799	1.502403	0.00209933	-2.469549	0.0010115
SM.C16:1	-0.329319	0.36471483	0.137652	0.69107536	-1.677868	0.0030054
PC.aa.C28:1	0.497961	0.2362651	-0.146295	0.71320958	-1.84345	0.00425661
Serotonin	-1.309419	0.0127778	-0.326219	0.48954433	1.867439	0.01213627
PC.aa.C36:1	0.434464	0.38771053	0.707405	0.14952168	-1.898897	0.01240534
lysoPC.a.C18:0	1.552868	0.0042796	0.708546	0.14460244	-1.808525	0.01553235
PC.aa.C36:2	0.239277	0.63215859	0.707496	0.14938503	-1.760378	0.01926578
PC.aa.C32:3	0.872059	0.1060994	0.385805	0.44603945	-1.732859	0.02710815
PC.ae.C44:5	-1.069698	0.0556154	-0.698752	0.18326069	1.712776	0.03210078

(A-B) Metabolites and corresponding statistics in which a significant age x diet interaction was observed in serum from younger (Y) and older (O) humans (n=6-7 per group). However, only C14:1 was significant at an FDR α=0.2. Box and whisker plots represent lower and upper quartile range and black line indicates the median. Dot plots overlaid on bar graphs represent individual data points.

Figure S2 (Related to Figures 2 and 3). BIOCRATES metabolomic analysis in rat brown adipose tissue with aging and DR.

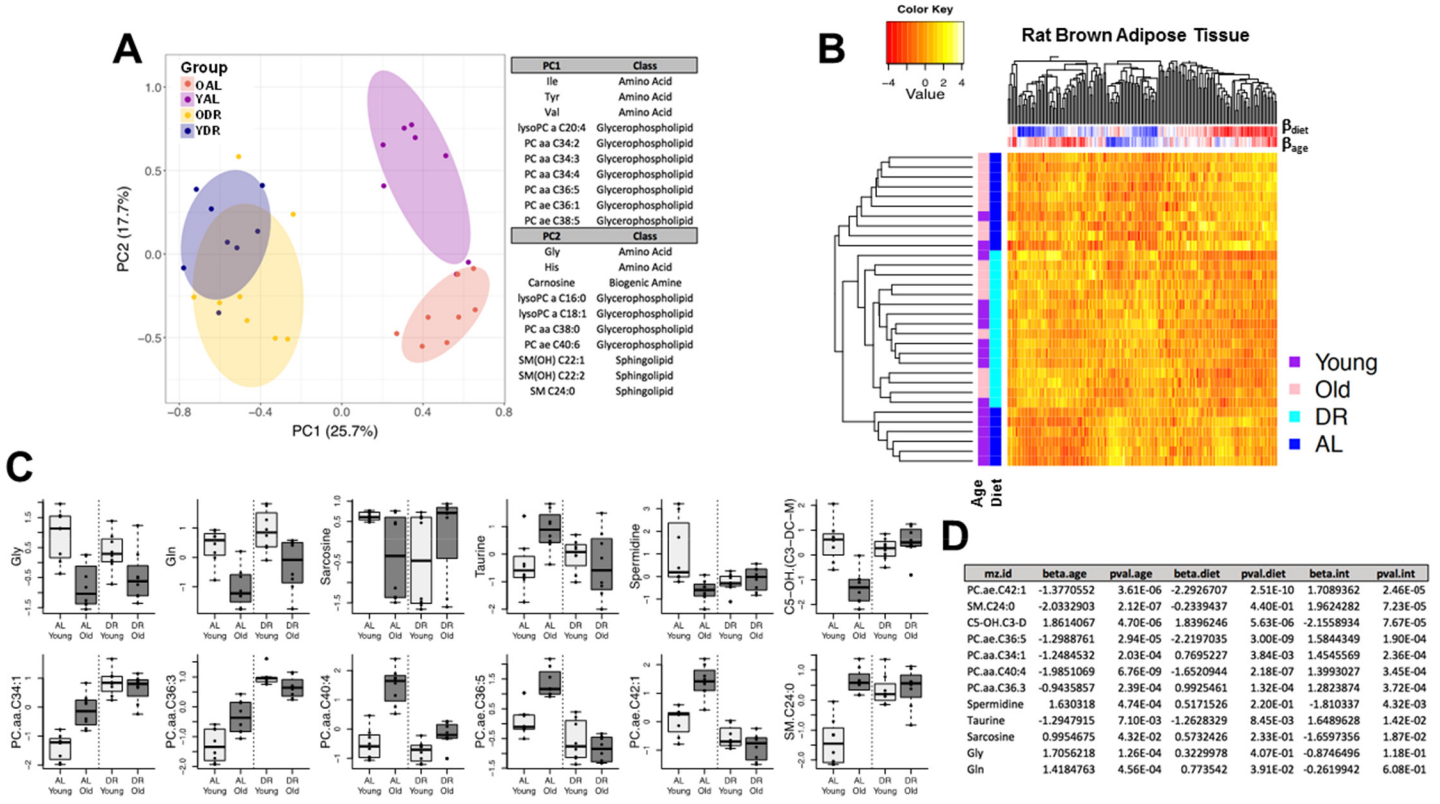

mz.id	beta.age	pval.age	beta.diet	pval.diet	beta.int	pval.int
PC.ae.C42:1	-1.3770552	3.61E-06	-2.2926707	2.51E-10	1.7089362	2.46E-05
SM.C24:0	-2.0332903	2.12E-07	-0.2339437	4.40E-01	1.9624282	7.23E-05
C5-OH.C3-D	1.8614067	4.70E-06	1.8396246	5.63E-06	-2.1558934	7.67E-05
PC.ae.C36:5	-1.2988761	2.94E-05	-2.2197035	3.00E-09	1.5844349	1.90E-04
PC.aa.C34:1	-1.2484532	2.03E-04	0.7695227	3.84E-03	1.4545569	2.36E-04
PC.aa.C40:4	-1.9851069	6.76E-09	-1.6520944	2.18E-07	1.3993027	3.45E-04
PC.aa.C36.3	-0.9435857	2.39E-04	0.9925461	1.32E-04	1.2823874	3.72E-04
Spermidine	1.630318	4.74E-04	0.5171526	2.20E-01	-1.810337	4.32E-03
Taurine	-1.2947915	7.10E-03	-1.2628329	8.45E-03	1.6489628	1.42E-02
Sarcosine	0.9954675	4.32E-02	0.5732426	2.33E-01	-1.6597356	1.87E-02
Gly	1.7056218	1.26E-04	0.3229978	4.07E-01	-0.8746496	1.18E-01
Gln	1.4184763	4.56E-04	0.773542	3.91E-02	-0.2619942	6.08E-01

(A) Similar to plasma, PC1 demonstrates a strong effect of diet on the BAT metabolome, with a much smaller effect of age, though some discrimination can be observed among YAL and OAL groups. In contrast to plasma, a robust reduction in glycerophospholipids, amino acids, and sphingolipids were observed with age, and were among the most discriminating classes of metabolites.

(B) Heatmap of all metabolites analyzed illustrating hierarchical clustering of BAT levels with age and diet.

(C-D) Plots and table indicate BAT metabolites in which a significant age x diet interaction was observed. In BAT, DR robustly counteracted age-related changes in several BAT metabolites, particularly glycerophoplipids, and tended to preserve Cit and His levels (FDR α=0.2), but not other amino acids reduced with age. Moreover, some effects of DR *per se* resembled effects observe with age, as was the case for PCaaC34:1, PCaa36:3, and SM.C24:0, and lower levels of spermidine (*n*=8 per group). Box and whisker plots represent lower and upper quartile range and highest and lowest observations, respectively, and the black line indicates the median. Dot plots overlaid on boxes represent individual data points.

Figure S3 (Related to Figures 2 and 3). BIOCRATES metabolomic analysis in rat skeletal muscle with aging and DR.

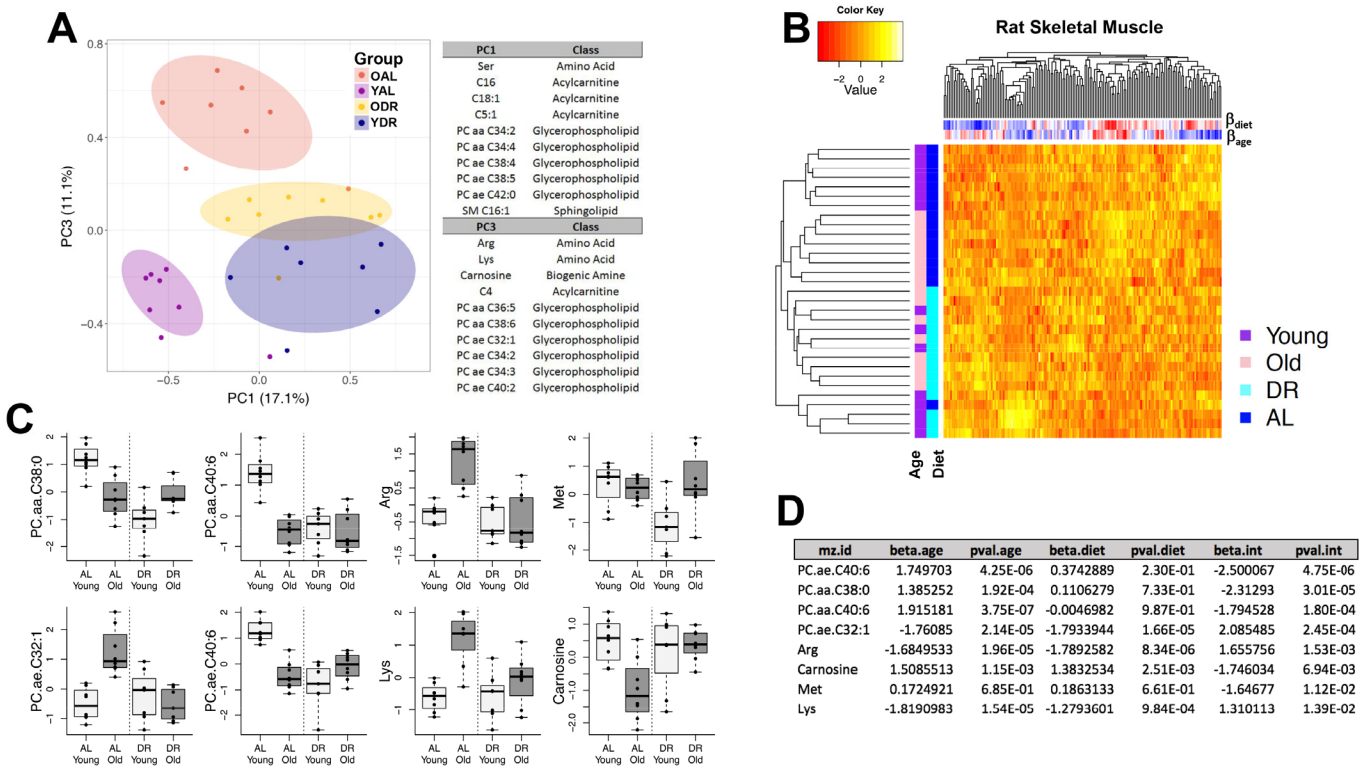

D

mz.id	beta.age	pval.age	beta.diet	pval.diet	beta.int	pval.int
PC.ae.C40:6	1.749703	4.25E-06	0.3742889	2.30E-01	-2.500067	4.75E-06
PC.aa.C38:0	1.385252	1.92E-04	0.1106279	7.33E-01	-2.31293	3.01E-05
PC.aa.C40:6	1.915181	3.75E-07	-0.0046982	9.87E-01	-1.794528	1.80E-04
PC.ae.C32:1	-1.76085	2.14E-05	-1.7933944	1.66E-05	2.085485	2.45E-04
Arg	-1.6849533	1.96E-05	-1.7892582	8.34E-06	1.655756	1.53E-03
Carnosine	1.5085513	1.15E-03	1.3832534	2.51E-03	-1.746034	6.94E-03
Met	0.1724921	6.85E-01	0.1863133	6.61E-01	-1.64677	1.12E-02
Lys	-1.8190983	1.54E-05	-1.2793601	9.84E-04	1.310113	1.39E-02

(A) PCA in SkM determined that PC3 metabolites revealed a strong effect of age on the metabolome, particularly glycerophospholipids, and to lesser extent amino acids and carnosine. However, DR attenuated the effect of age on the metabolomics profile in this tissue.

(B) Heatmap of all metabolites analyzed illustrating hierarchical clustering of SkM levels with age and diet.

(C-D) Plots and table indicate a representative number of SkM metabolites in which a significant diet x age interaction was observed (*n*=8 per group). Lifelong DR protected against perturbations to some metabolites, including Arg Lys, and carnosine. Interestingly, while DR was found to attenuate age-related changes in some glycerophospholipids perturbed by age, in other cases, the effect of DR closely resembled the effect of age on metabolite levels, as was the case for PCaaC38:0, PCaaC40:6 and PCaeC40:6. Box and whisker plots represent lower and upper quartile range and highest and lowest observations, respectively, and the black line indicates the median. Dot plots overlaid on boxes represent individual data points.

Figure S4 (Related to Figures 2 and 3). BIOCRATES metabolomic analysis in rat liver with aging and DR.

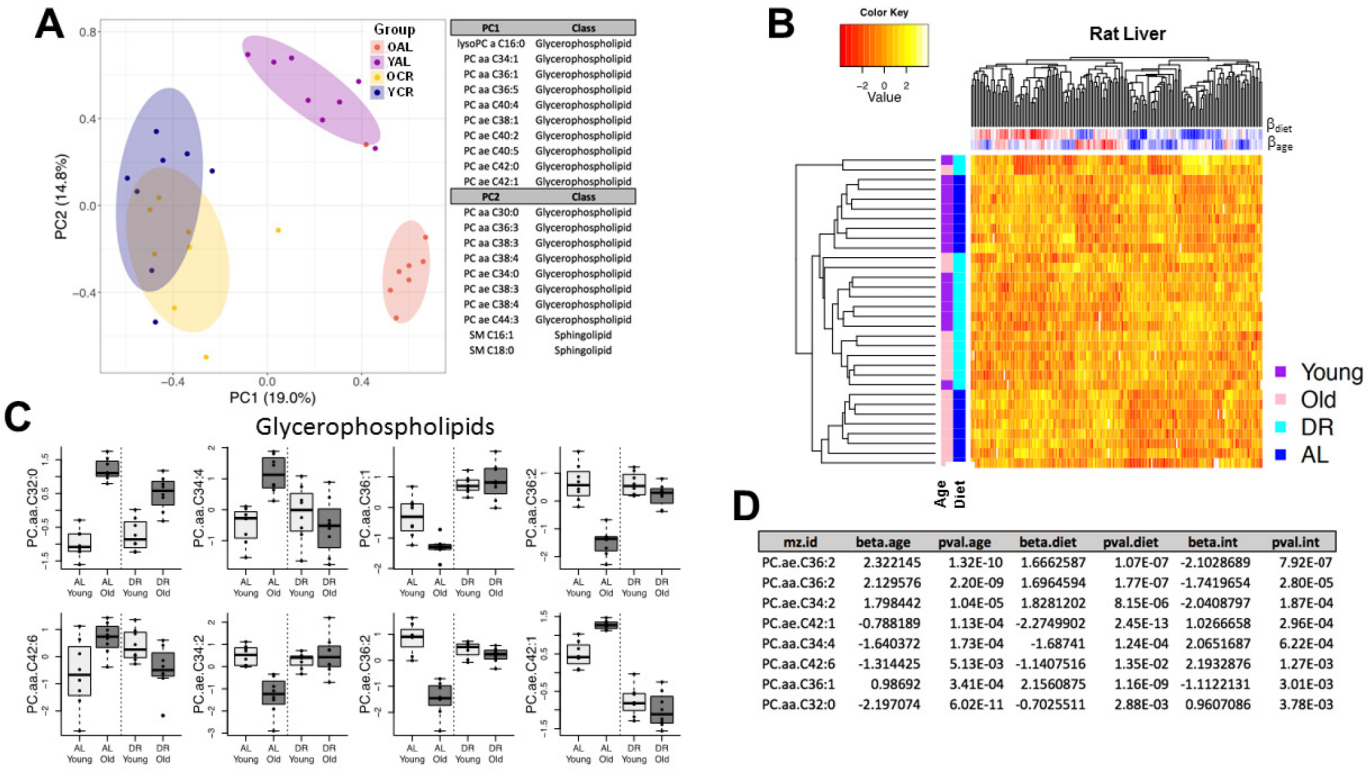

D

mz.id	beta.age	pval.age	beta.diet	pval.diet	beta.int	pval.int
PC.ae.C36:2	2.322145	1.32E-10	1.6662587	1.07E-07	-2.1028689	7.92E-07
PC.aa.C36:2	2.129576	2.20E-09	1.6964594	1.77E-07	-1.7419654	2.80E-05
PC.ae.C34:2	1.798442	1.04E-05	1.8281202	8.15E-06	-2.0408797	1.87E-04
PC.ae.C42:1	-0.788189	1.13E-04	-2.2749902	2.45E-13	1.0266658	2.96E-04
PC.aa.C34:4	-1.640372	1.73E-04	-1.68741	1.24E-04	2.0651687	6.22E-04
PC.aa.C42:6	-1.314425	5.13E-03	-1.1407516	1.35E-02	2.1932876	1.27E-03
PC.aa.C36:1	0.98692	3.41E-04	2.1560875	1.16E-09	-1.1122131	3.01E-03
PC.aa.C32:0	-2.197074	6.02E-11	-0.7025511	2.88E-03	0.9607086	3.78E-03

(A) Metabolites comprising PC2 in liver confirmed distinct clustering by age, which was mainly driven by glycerophospholipids. However, a clear diet x age interaction is also present, as evidenced by high overlap of YDR and ODR groups.

(B) Heatmap of all metabolites analyzed illustrating hierarchical clustering of SkM levels with age and diet.

(C-D) Plots and table indicate a representative number of liver metabolites, namely glycerophospholipids, in which a significant diet x age interaction was observed (*n*=8 per group). DR generally opposed age-related changes to liver glycerophospholipids. Box and whisker plots represent lower and upper quartile range and highest and lowest observations, respectively, and the black line indicates the median. Dot plots overlaid on boxes represent individual data points.

Figure S5 (Related to Figure 5). Effect of a sarcosine-supplemented diet on the aging rat metabolome.

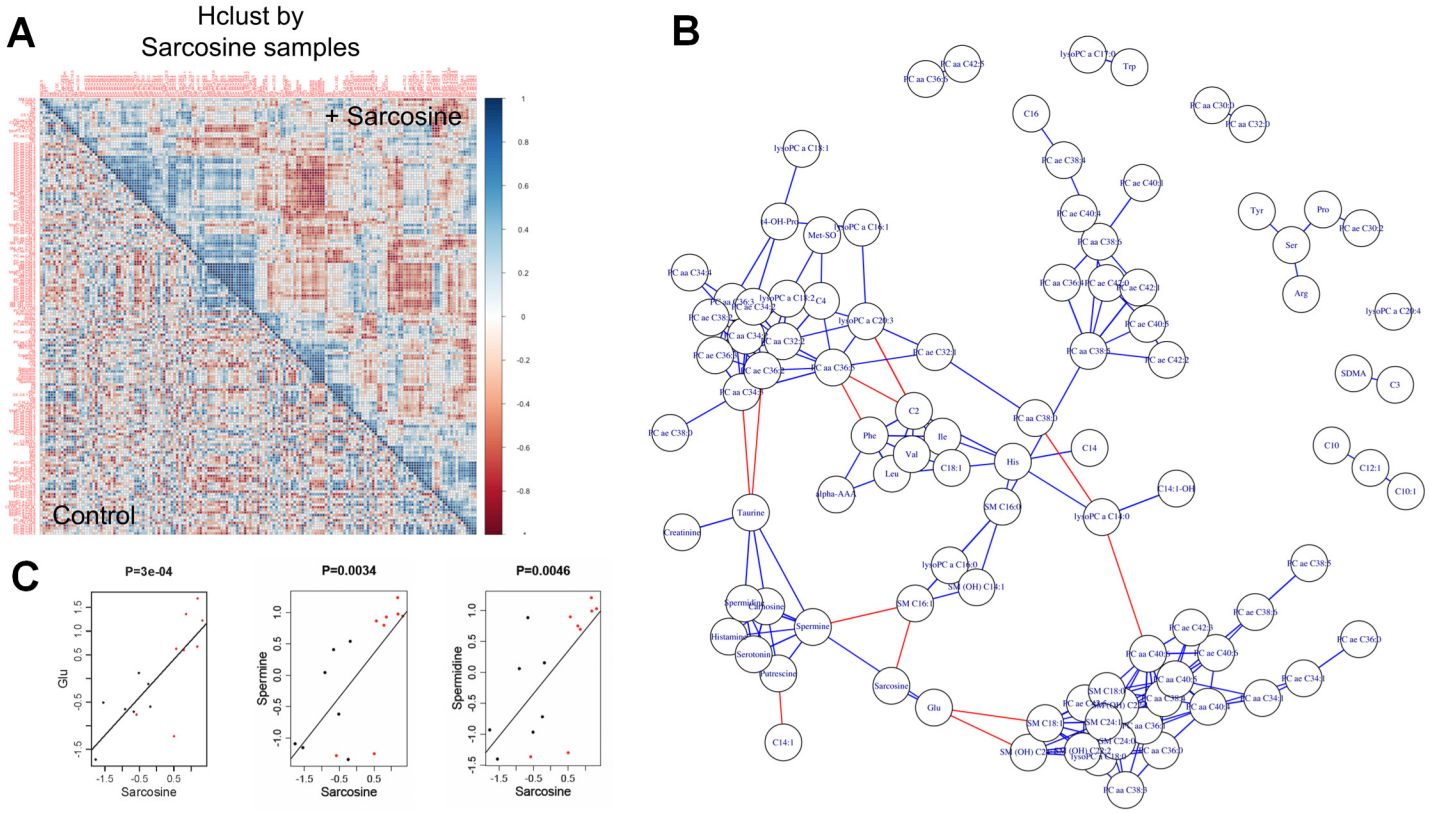

(A) Heat cluster map showing clear, extensive alterations to the old rat plasma metabolome, as determined by the BIOCRATES p180 assay, with 8 wks sarcosine supplementation (*n*=8 per group).

(B) Detailed correlation map of plasma sarcosine with other metabolites demonstrates a strong association with glutamate and high 'betweenness' score, linking nodes of amino acids, biogenic amines and lipid metabolites.

(C) Plasma sarcosine was positively correlated most strongly with circulating levels of Glu (P<0.001), but was also associated with spermine and spermidine in control and sarcosine-supplemented rats (FDR cutoff=0.12).

Figure S6 (Related to Figure 5). Effect of sarcosine on one-carbon metabolites and regulation by timing and nutrient status *in vivo*

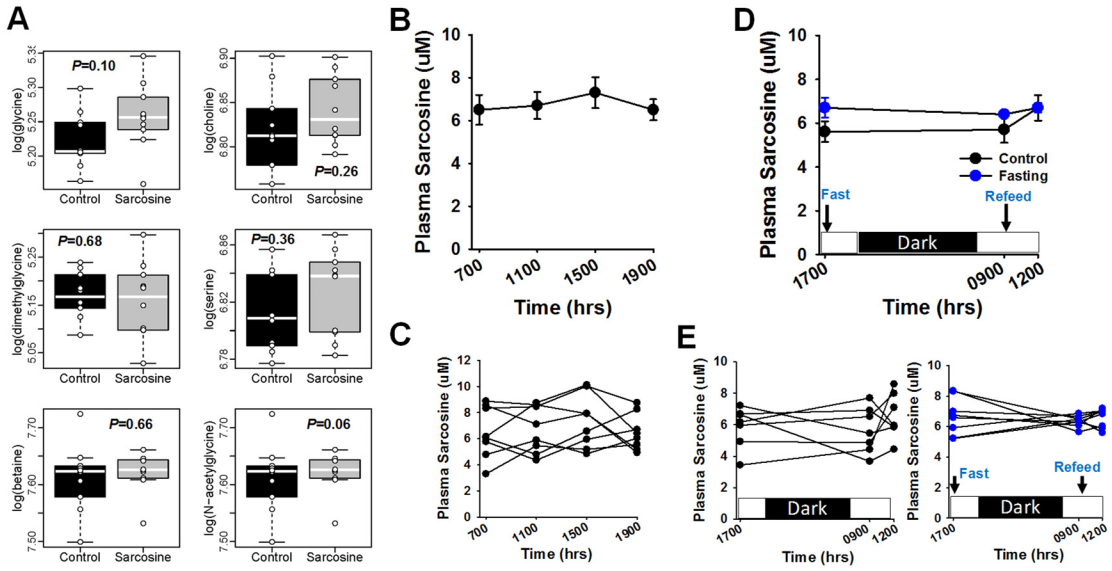

(A) Targeted metabolomics analysis was performed for 11 (only 7 detected) one-carbon metabolites in plasma obtained from older FBN rats (~25 mo) following 4 wks of sarcosine feeding. While Met levels were significantly reduced (see Fig. 5J), glycine and N-acetylglycine tended to be increased by sarcosine feeding. Meanwhile, no effect was observed for choline, dimethylglycine, serine or betaine levels (*n*=10 per group).

(B-C) To determine if sarcosine is diurunally regulated, catheterized animals remained in their home cage and had continuous access to food and water throughout the day. Venous samples were collected from awake, unstressed rats at 0700, 1100, 1500 and 1900hr, respectively, and plasma sarcosine was assessed with a fluorescence-based detection coupled assay. Time of day had no effect on sarcosine, as determined by repeated measures analysis of sarcosine levels, nor were there any discernable trends in individual animals (*n*=8).

(D-E) Effect of feeding status was also assessed on sarcosine levels in male FBN rats. As can be observed, sarcosine levels were not different between fed, fasted or refed conditions in the same animals (blue circles), nor did levels differ from a fed diurnal control group (black circles) at any timepoint. This is further demonstrated by lack of discernable trends in sarcosine levels in individual animals across time and treatment (*n*=7 group). Box and whisker plots represent lower and upper quartile range and highest and lowest observations, respectively, and the white line indicates the median. Dot plots overlaid on boxes represent individual data points. Lines and symbols represent mean±SEM.

Figure S7 (Related to Figures 6 and 7). Effect of sarcosine on autophagy in cultured cells and *in vivo*.

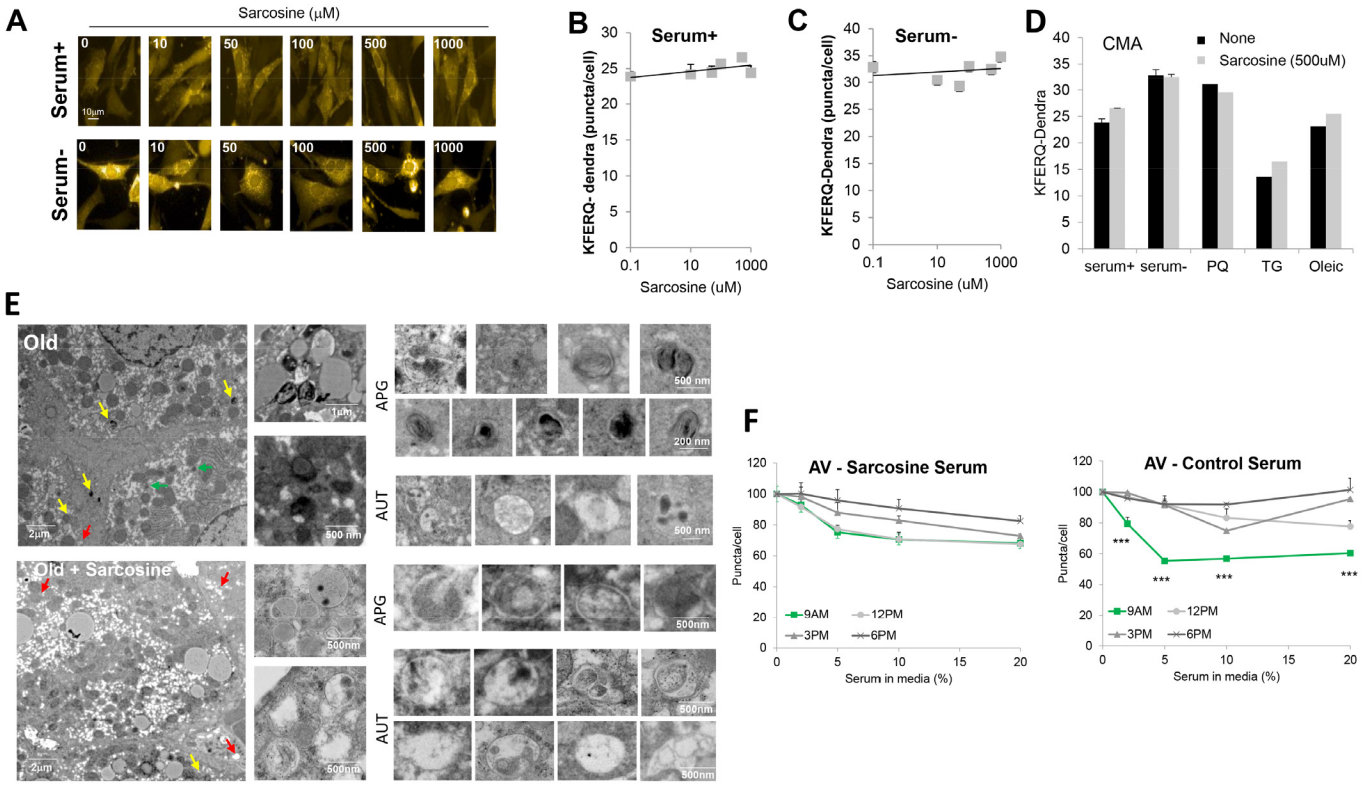

(A) Cultured mouse fibroblasts (NIH3T3 cells) expressing the CMA reporter KFERQ-PS-Dendra were photoswitched and exposed to the indicated concentrations of sarcosine for 16h in absence or presence of serum. CMA was analyzed as the number of puncta per cell at the end of the incubation time. Representative images of cells treated with different concentrations of sarcosine in presence or absence of serum.

(B-C) Quantification of the number of puncta per cells at the indicated sarcosine concentrations in cells maintained in serum supplemented or serum free media (n>2,500 cells).

(D) Effect of the indicated treatments on CMA activity of mouse fibroblasts in culture untreated (None) or supplemented with 500 μM sarcosine (n>2,500 cells). No significant differences were observed for CMA with addition of sarcosine to cell culture media.

(E) Rat liver ultrastructure following a short-term (10 days) dietary sarcosine treatment. Images at low (left) and high magnification (right) showing autophagic/lysosomal compartments in untreated (A) or sarcosine treated (B) livers. Inserts on the right show examples of autophagosomes (APG) and autolysosomes (AUT) in each group. Arrows mark lysosomes (green), autolysosomes (red) and autophagosomes (yellow). All smaller panels on the right are shown at the same magnification.

F) Effect of old control and sarcosine-treated rat serum on autophagy (*n*=3 per group). In addition to collecting serum at 0900h (see Fig. 7C), serum was also obtained from the same animals via i.v. catheter at 1200h, 1500h (3p) and 1800h (6p), and heat-inactivated prior to performing experiments. Remarkably, while addition of serum obtained from sarcosine-supplemented rats at 0900h to the culture media of NIH3T3 cells led to less inhibition of autophagy, as demonstrated by autophagic vacuoles (AV, mcherry+ vesicles), addition of serum obtained at later time points were not different from control. Data were quantified using high content microscopy (n>2,500 cells). Bars and lines indicated mean±SEM. Significantly different from control serum obtained at later time points, ***P<0.001.